Lappeenranta-Lahti University of Technology LUT
School of Engineering Science
Technical Physics
Master's Programme in Computational Engineering and Technical Physics

Iuliia Zhelezova

SINGLE-MODE ALL GLASS DELIVERY FIBER FOR ULTRA-HIGH -POWER LASER SYSTEM

Examiners: Professor Erkki Lähderanta
Senior Research Fellow, D.Sc. (Tech.) Regina Gumenyuk

Supervisors: Professor Erkki Lähderanta
Senior Research Fellow, D.Sc. (Tech.) Regina Gumenyuk

ABSTRACT

Lappeenranta-Lahti University of Technology LUT
School of Engineering Science
Technical Physics
Master's Programme in Computational Engineering and Technical Physics

Iuliia Zhelezova

Single-mode all glass delivery fiber for ultra-high-power laser system

Master’s Thesis

92 pages, 50 figures, 14 table

Examiners: Professor Erkki Lähderanta
Senior Research Fellow, D.Sc. (Tech.) Regina Gumenyuk

Keywords: Large mode area fiber, ultra-high power laser system, stimulated Raman scattering, delivery fiber

This work is devoted to investigation of a novel large-mode area (LMA) optical fiber developed for delivery of ultra-short highly intense pulses over several meters’ length. This subject is a bottleneck of the current ultra-short pulsed high-power laser systems and represent important constituent for future progress of industrial lasers and laser-driven applications. The novel optical fiber has a complex all-glass W-type structure ensured fundamental mode confinement and low loss propagation. For the experimental investigation six samples of the delivery fiber with the different geometry has been fabricated and investigated.

This thesis describes the characterization of the main fiber parameters such as sensitivity to the bending, mode field diameter, divergence and beam quality. It includes the details of the

experimental setup and the measurement results. The optical launch system has been calculated and realized based on laboratory available lenses.

The investigation revealed a strong fundamental mode confinement in the fiber core resulted in low bending sensitivity and high beam quality up to 15 m length of the fiber. The maximum coupling efficiency was as high as 50 % leaving a small room for further possible improvement.

TABLE OF CONTENTS

LIST OF ABBREVIATIONS

BBP	Beam parameter product
CCD	Charge-coupled device
CPA	Chirped pulse amplification
CW	Continuous-wave
Er^{3+}	Erbium
FWHM	Full width at half-maximum
LMA	Large-mode area
MFD	Mode field diameter
MOF	Microstructured optical fiber
NA	Numerical aperture
Nd^{3+}	Neodymium
PBG	Photonic bandgap
Pr^{3+}	Praseodymium
SBS	Stimulated Brillouin scattering
Tm^{3+}	Thulium
TIR	Total intermal reflection
Yb^{3+}	Ytterbium

1. INTRODUCTION

A LASER is an abbreviation for Light Amplification due to Stimulated Emission of Radiation. It is a device emitting coherent light through the process of stimulated emission taken place in molecules or atoms. Laser radiation typically covers a relatively narrow wavelength range specified in visible, infrared or ultraviolet spectral range [1].

The main characteristics of the laser beam are monochromaticity, coherence and collimation. Monochromaticity, i.e. maintaining any color of a certain wavelength. In other words, this is the laser ability to emit light in a restricted wavelength range. Coherence, i.e. the light waves of a laser beam have the same energy, frequency or wavelength; thus, these waves coincide in the spatial and temporal phases. Due to this property, the laser beam can be focused to a point of incredibly small size, and the energy in its focus has a huge density. Collimation, i.e. all photons move in the same direction. This means that the laser beam travels with low divergence over long distances [2].

The properties of laser radiation are unique. Multiplying by high power, it turned lasers into an indispensable tool for various fields of science and technology. The easily achievable high density of radiation energy allows controllable and high precision variable material treatments (cutting, welding, surface structuring, soldering, and engraving) [3]. Exact control of the heating zone allows processing of materials that cannot be realized by conventional methods (for example, ceramic and metal). When laser is processing of materials, they are not subjected to mechanical stress since the heating zone is small, so only insignificant thermal deformations occur. Therefore, laser processing is characterized by high accuracy and productivity. The ability of the laser beam to be focused on tiny point, having a diameter of the order of a micron, is exploited for engraving microcircuits. Second great feature of a laser beam is its perfect directness giving the possibility to use it as the most accurate "line" in construction. Also in construction and geodesy [4] pulsed lasers are utilized for measurement of huge distances on the ground by detecting the time during which the light pulse travels from one point to another. In addition, using a laser beam, CDs are recorded and played back with sounds, music, images, photos and films. The recording industry, having received such an instrument, has taken a giant step forward. Laser

technologies are widely used both in surgery and for therapeutic purposes [5]. For example, due to its unique capabilities, the laser beam can be easily directed through the eye pupil and the laser can do “welding” the exfoliated retina, and correct existing defects in the inaccessible area of the fundus. For military purposes, the range of application of lasers is very large. For example, they are used in intelligence, i.e. to search for targets and communications [6].

Solid-state laser systems are of most interest since they are currently the most powerful lasers in the world [7]. These devices are easy to maintain and capable of generating high power energy. Laser radiation requires the so-called "active medium". Radiation can occur only in that part. For solid-state lasers, a solid substance acts as an active medium (e.g. activated dielectric crystals or glasses). This is their key difference from other types of lasers (gas lasers, liquid lasers etc.). A variety of solid-state lasers includes fiber lasers [8], disk lasers [9] and bulk-lasers [10]. A more specific example of a bulk laser is a rod laser [11]. When working with solid-state lasers, three main operating modes are realized [12]: continuous mode, pulsed mode and quasi-continuous mode. In the continuous mode, optical energy is emitted continuously for a certain period. In the pulsed mode, single or regularly repeated pulses of laser radiation are generated. In quasi-continuous mode, the laser operates at certain intervals that are short enough to significantly reduce thermal effects, but long enough to consider the laser almost continuous. Pulse mode are realized by mode-locked [13] and Q-switched mode [10] techniques. Mode-locked is a technique in optics by which a laser can be made to produce pulses of light of extremely short duration, approximately picoseconds or femtoseconds. The Q-switched mode allows the generation of light pulses with extremely high energy power in the nanosecond range, far exceeding what would be produced by the same laser if it were to operate in the quasi-continuous wave mode (with constant power).

This thesis is structured in the following way. Chapter 2 covers the current state-of-the-art of solid-state lasers. Chapter 3 describes operation mode of the modern high-power lasers. Chapter 4 presents the mechanisms of light confinement and propagation in an optical fiber and gives an overview of the current large-mode area fiber technology. Chapter 5 describes the nonlinear effects following the light propagation in optical fibers. Chapter 6 is denoted

to experimental characterization of novel W-type large mode area fiber. Finally, chapter 7 concludes the main results of the thesis.

2. HIGH POWER SOLID-STATE LASERS

Ultra-high-power laser systems remain at the forefront in many scientific spheres, and progress in the development of these systems continues to pave the way for new and spectacular areas of the scientific world. Most notably, over the past decade, there has been a leap in laser performance, which has resulted in a significant increasing in the average power of laser systems, opening up new breath-taking possibilities [14].

Bulk multi-stage laser amplifiers can produce energetic pulses of the millijoule-class in the near infrared wavelength region having a duration of several tens of femtoseconds and gigawatts/petawatts of peak power. However, a laser design is limited in the average power by an order of several tens of watts due to weak heat dissipation. A more advantageous option for heat dissipation in high-power laser systems is exhibited by fiber and disk lasers whose peak power reaches the gigawatt range and the average power exceeds the kilowatt range, as can be seen from Figure 1 [14].

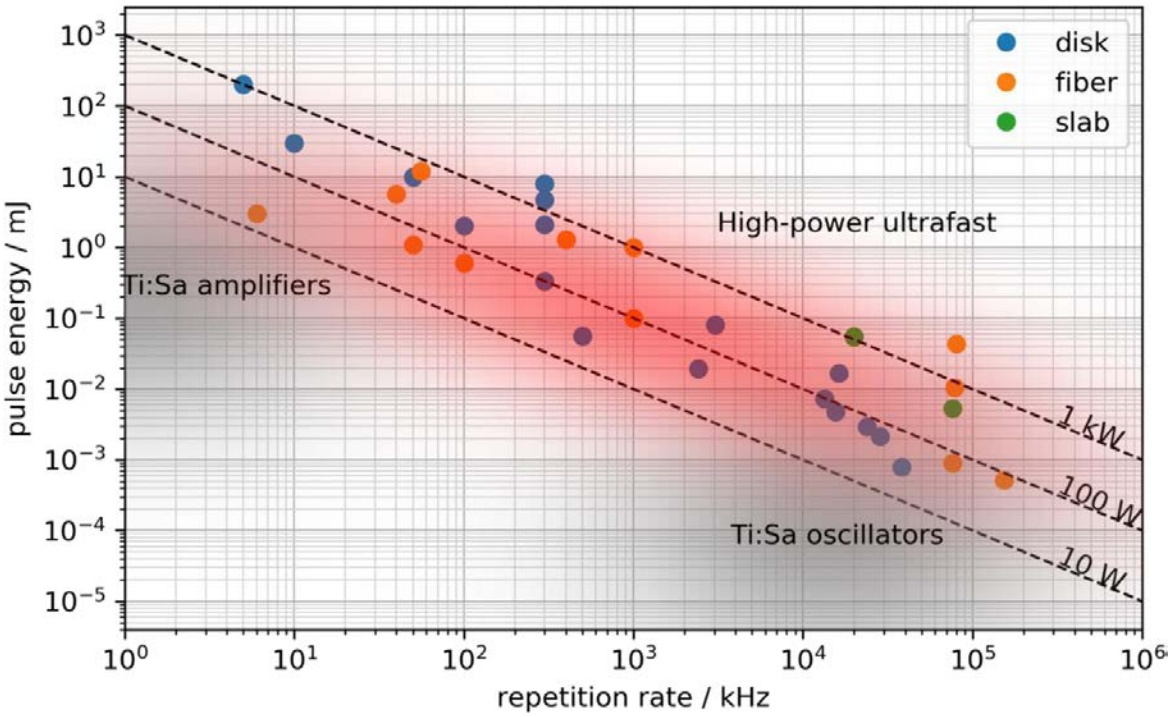

Fig.1 State-of-the-art for ultra-high power solid-state lasers based on different geometries [14].

Further, in sections 2.1-2.3 we will focus deeply on the review of modern high-power solid-state laser systems: fiber-based, disk and bulk types.

2.1 Fiber lasers

Optical fibers are the main components of fiber optics and they play a significant role in the field of Photonics. They are optical waveguides, which are usually made of any glass, can potentially be very long (hundreds of kilometers) and, unlike other waveguides, quite flexible. Although glass is generally quite brittle, thin quartz fibers protected by a polymer coating can be bent, for instance, around the finger without breaking [15]. The most popular material used for optical fibers is silica (quartz glass or SiO_2) due to its potential for extremely low propagation loss and its surprisingly high mechanical tensile and even bending strength [10].

The fiber laser is a powerful machine for creating single-mode radiation with the highest possible performance and quality characteristics, in which the active medium and the resonator are elements of an optical fiber. The simple schematic of fiber laser is shown in Figure 2. The length of the optical fiber can range from a couple of meters to several tens, or even hundred meters, therefore, to optimize the space, it is twisted with rings and laid on the surface of the equipment. In most cases, the gain medium is a fiber doped with rare-earth ions such as erbium (Er^{3+}), neodymium (Nd^{3+}), ytterbium (Yb^{3+}), thulium (Tm^{3+}), or praseodymium (Pr^{3+}). The system of fiber lasers consists of main parts: pump system (laser diodes), which pump the optical element with energy, mirrors acting as a resonator to increase the power of laser radiation, and an active optical fiber. Inside the optical fiber, there is a thin light-conducting core that is made of transparent quartz. For stable operation and eliminating the likelihood of damage, the fiber is enclosed in a polymer cladding and an external protective coating [16].

Femtosecond ytterbium-based fiber optical lasers are promising instruments for amplification due to their high optical quality of emitting radiation, small dimensions, wide spectral bandwidth of ytterbium silicon dioxide and convenient integration into fiber lines, as well as the possibility of tuning the wavelength in a wide range. In the chirped pulse amplification method (CPA method), it is possible to achieve a pulse energy of several mJ

and a surprisingly record peak power of the order of several tens of GW with an average power from several hundred watts up to kilowatts [17]. A more detailed description of the CPA method is presented in the section 3.2.2. The disadvantage of such lasers is the limitation of peak power due to the propagation of light in a limited small area - in the core of a fiber, which results in non-linear effects due to the high radiation density [18].

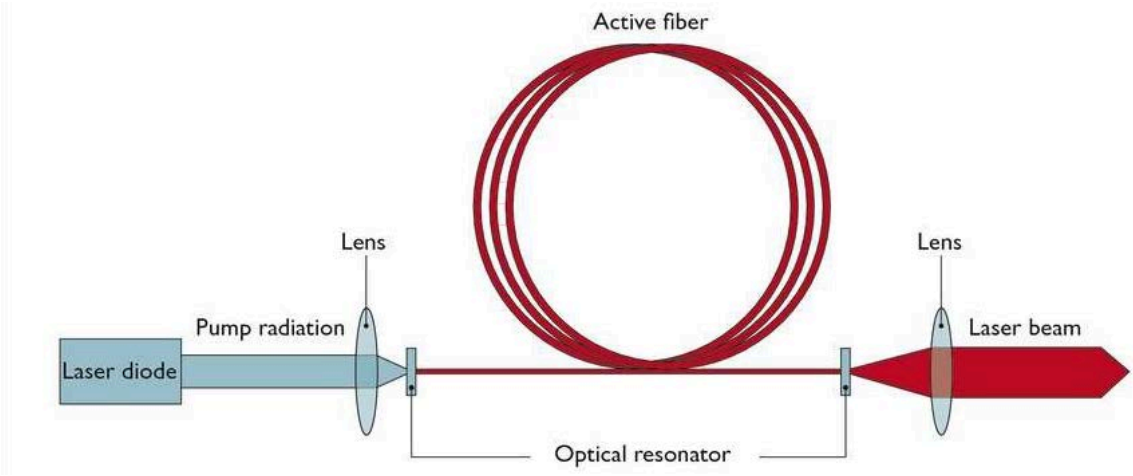

Fig. 2. Schematic representation of fiber laser components [15].

2.2 Disk lasers

A disk laser with a multi-pass pump system comprises a parabolic mirror with an optical axis and a hole near the axis [19]. An active lasing material (thin disk crystal on heat sink in Fig. 3) are placed at the focal length from the parabolic mirror. Also disk laser contains laser pump diode with fiber output and an optical system forming a collimated beam of laser diode radiation and directing this beam to a parabolic mirror parallel to the optical axis. A set of reflective prisms is located around the active plate and an external partially transmitting mirror located on the optical axis behind the hole in the parabolic mirror and forming, together with the mirror coating of the active plate, an optical disk laser resonator. The disk laser setup is shown in the Figure 3.

The main advantages of thin disk lasers are, firstly, excellent heat dissipation, and secondly, the geometry of the disk supporting ultra-fast operation. Disk lasers are noteworthy in that their large mode areas on an amplifying medium, as well as the short propagation distances of pulses through this amplifying medium, are beneficial for small

nonlinear phenomena at very high pulse energies. Multi-pass disk laser systems are extremely successful in achieving an average output power of up to kilowatts with pulse energies ranging from a few millijoules to a level of several hundred millijoules. Moreover, the geometry of such disk amplifiers offers a unique opportunity for implementation of mode-locked technique at a very high level of average power, operating with a repetition frequency of several MHz and a pulse energy of about a dozen microjoules. With sufficient pump, it is possible to achieve Joule level for the pulse energy. To reach even higher energies, a method called chirped pulse amplification can be applied (CPA method is presented in section 3.2.2) enabling the order of several GW for the peak power [14].

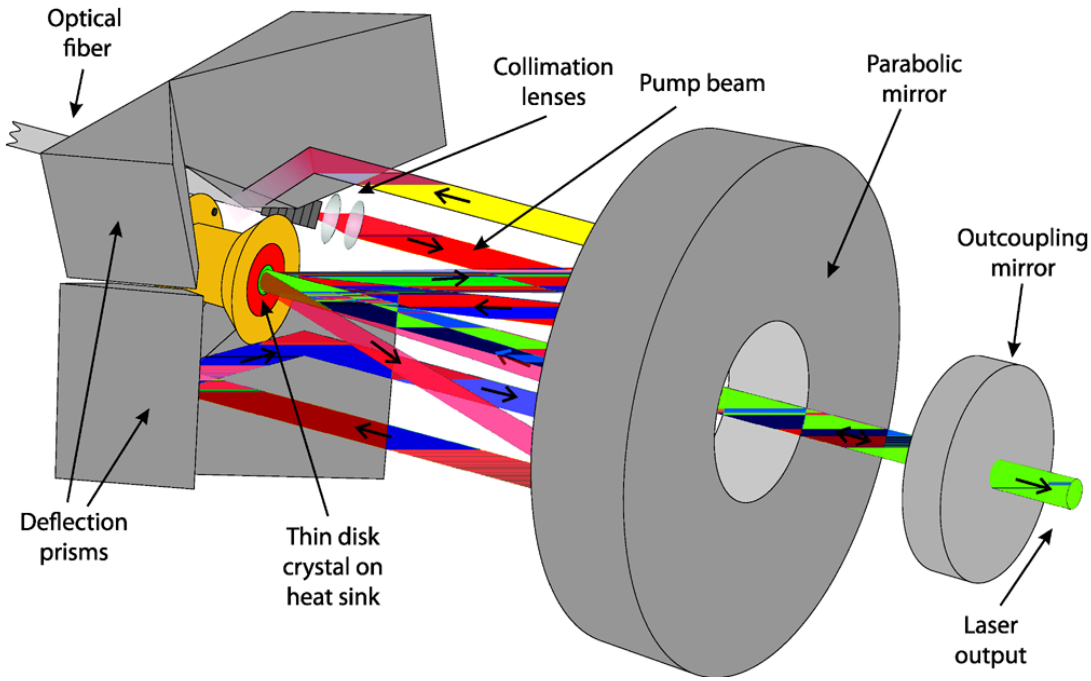

Fig. 3. Schematic setup of a disk laser configuration [19].

2.3 Bulk (rod) lasers

The bulk laser relates to a solid-state laser with a volumetric piece of a doped crystal or glass as an amplifying medium. In most cases, the amplifying medium is doped with rare-earth ions or transition metal ions [10]. The experimental setup of the bulk laser is shown in the Figure 4.

Due to the fact that the waveguide structure is absent, so that the beam propagates in the free space localized between the optical components, the radius of the beam in the amplifying medium is essentially determined not by the amplifying medium, but by the design of the laser resonator. The laser resonator of a bulk laser is in most cases formed of laser mirrors located around a crystal (or glass), with an air space between them. The pulsed laser cavity incorporates an active Q-switch element, an optical modulator, which will be discussed more detailed in the following sections.

The main advantages of bulk lasers are their preference for devices operating with high peak power; bulk lasers can use pump sources with very low beam quality. In addition, bulk lasers are more flexible, i.e. in laboratory installations, it is relatively easy to add or replace optical elements [20].

With a combination of extraction methods during pumping and thin-disk technology, it became possible for the laser system to obtain ultra-high peak power at the level of several petawatts. The extraction method during pumping consists in temporarily distributing the pump in a multi-pass amplifier operating in a state close to saturation, so that the losses do not have time to significantly increase between passes of the laser pulse of the source through the active medium. The most promising crystal for achieving such a high power is titanium-sapphire due to such remarkable features as a wide spectrum of radiation, a good thermal conductivity and a high concentration density of active ions. With an optical energy of about several joules and a pulse duration of several tens of femtoseconds, it is possible to obtain an amazing result for a peak laser power of several hundred terawatts and an average power close to the kilowatt range at a repetition frequency of 100 Hz [21].

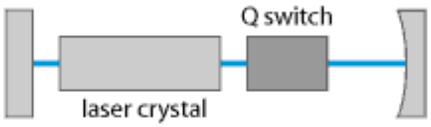

Fig. 4. Bulk laser experimental setup [10].

Solid-state rod lasers are doped crystal lasers in the form of a rod acting as an amplifying medium. In this type of laser, the rod has a cylindrical shape [10]. The ends of the rod are usually either perpendicular to the axis of the beam, or are located at a Brewster angle to suppress spurious reflections and to ensure a stable linear polarization. An example of a rod laser construction is shown in Figure 5 (LD is a laser diode module on Fig. 5).

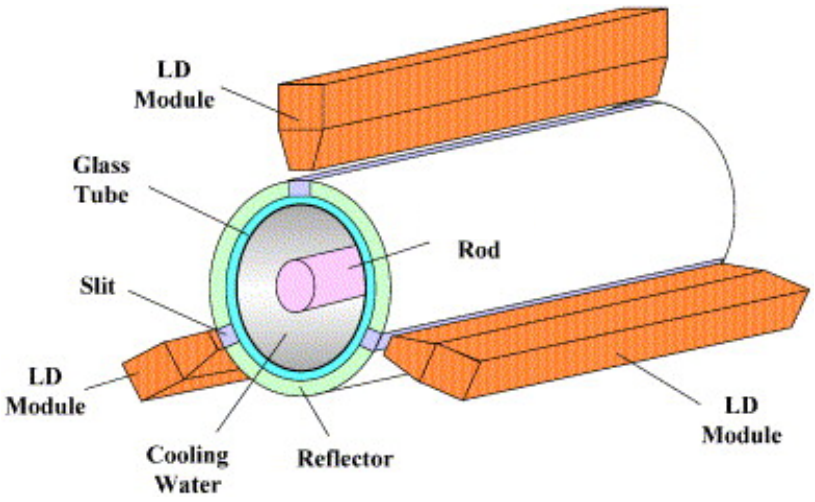

Fig. 5. Schematic diagram of a Rod laser [11].

In a rod laser design, a laser resonator may include one or more rods. When using multiple rods, the laser gain is higher, which provides a higher level of output coupling.

Any solid-state lasers can be designed to operate in a certain regime such as continuous-wave, quasi-continuous wave and pulsed regimes, which are discussed in detail in the next section.

3. OPERATION REGIMES FOR SOLID-STATE LASERS

The modern high-power solid-state lasers are designed to operate in different regimes such as continuous-wave, quasi continuous-wave and pulsed regime. Each regime is used in specific application area. Continuous wave high-power lasers are working in simple material processing (cutting, surface cleaning). Quasi continuous-wave laser systems are in demand for metal welding. Pulse regime are used for mode delicate processing such as drilling, ablation and cutting of delicate material. Especially, ultra-short pulsed lasers have attracted large interest due to possibility to realize “cold ablation” technique resulted in high speed and precision. This chapter describes the definitions and features of each operation regime.

3.1 Continuous-wave and quasi-continuous-wave regimes

Continuous-wave (CW) regime of operation of light sources means that it works continuously, it is not pulsed [10], [22]. For a laser, continuous-wave regime implies that the CW mode will distribute emission evenly throughout the period, that is, stable radiation will be ensured (Fig. 6 (a)). Radiation can occur in a single-frequency mode or in several modes. If the mode is emitted by the laser having a duration of 0.25 s or more, this laser is called a continuous-wave laser [23]. The CW regime in the modern high-power lasers has several variations. Figure 6 below shows the different output power behaviors for the continuous-wave regime of operation.

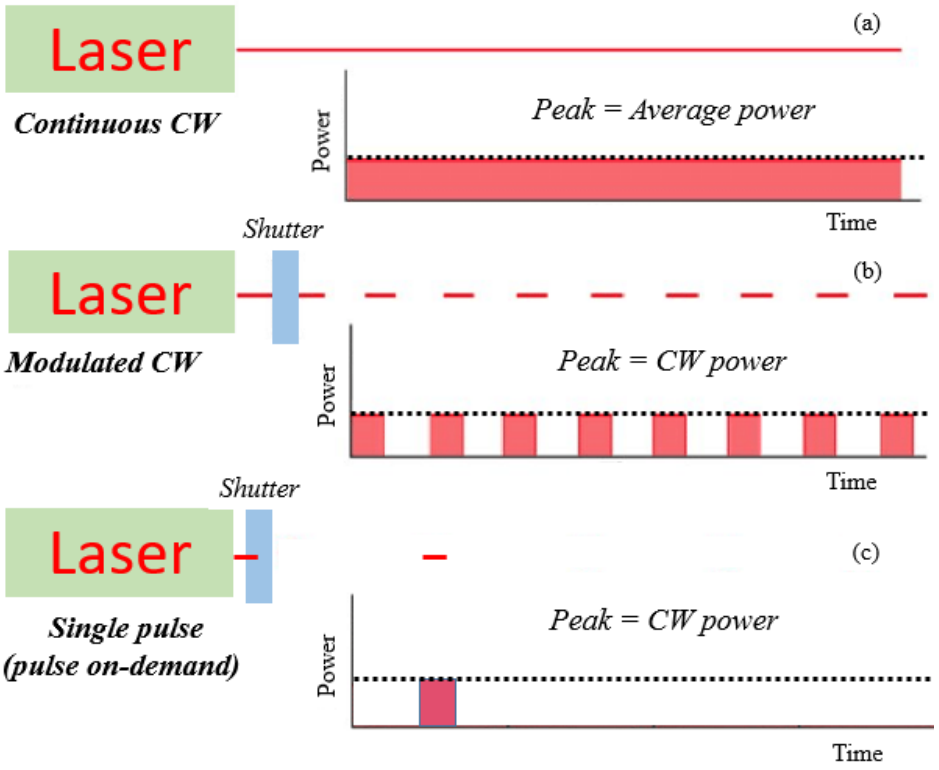

Fig. 6. Representation of different output power behaviors for the continuous-wave (CW) regime of operation (a) a continuous CW, (b) a modulated CW and (c) a single pulse (pulse on-demand).

Figure 6 represents schematically the output performance of classical continuous wave regime, and its variations with the help of the output shutter. The role of the shutter is to control the time frame when the laser light will be delivered. Without a shutter, a continuous-wave regime will take place; applying the shutter becomes possible to implement a modulated CW regime and a single pulse. It might happen once a time (pulse-on demand regime) or periodically (modulated CW). The pulse-on-demand and modulated CW regimes are referred to quasi-CW operation. The distinctive features of these regimes is that the "peak" power of the modulated pulse does not exceed the average power (similar as for continuous CW). The variation in time of continuous wave brings certain flexibility to the laser-driven applications. It is used when the short pulses are not needed but the operation requires periodical switching on/off the laser light.

3.2 Pulsed regime

In the pulsed laser regime the radiation of light flashes so that emission is separated in time [24].

The main parameters of the pulsed laser mode are repetition rate f_{rep}, pulse duration τ, pulse energy E, average power P_{avg} and peak power P_{peak}. These parameters are presented in the Figure 7 [25].

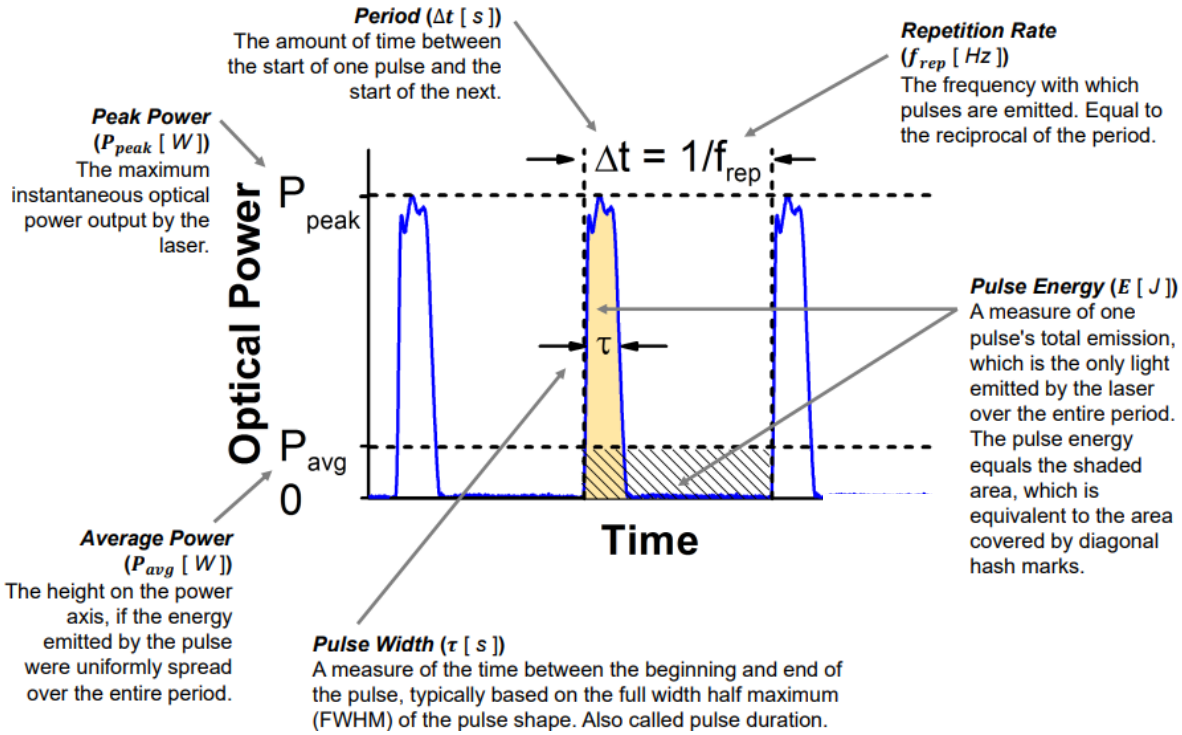

Fig. 7. The main parameters of the pulsed laser regime [25].

When the laser operates in pulsed regime, the number of pulses per second or the repetition rate of a regular pulse sequence is called the pulse repetition rate f_{rep}. This term is defined as the number of pulses emitted by the laser source per second or the inverse time distance between pulses, as presented in equation:

$$f_{rep} = \frac{1}{\Delta t}, \tag{1}$$

where Δt is the time between the beginning of one pulse and the beginning of the next one [25].

Knowing the numerical value of the pulse repetition rate f_{rep}, it is possible to calculate an important characteristic of the laser operation in the pulsed regime, the pulse energy E. The concept of pulse energy E can be explained as the total content of the optical energy of a pulse, in other words, it is the integral of optical power over time.

For a sequence of regularly repeating pulses, the pulse energy E can be found by the formula 2, i.e. by dividing the optical average power P_{avg} on the pulse repetition rate f_{rep} [25]:

$$E = \frac{P_{avg}}{f_{rep}} = P_{avg}\,\Delta t\ . \tag{2}$$

A schematic representation of the pulse energy E is shown in the Figure 7. The pulse energy E is equal to the shaded area, which is equivalent to the area covered by diagonal hash marks.

Second important parameters of the laser operation in the pulsed regime is the peak power P_{peak}. The peak power P_{peak} is the maximum instantaneous optical power of a laser during a single pulse; but since the laser turns off at the required time intervals, the average power P_{avg} will be less than the peak power P_{peak}. In other words, average power P_{avg} is the height on the power axis if the energy emitted by the pulse was evenly distributed throughout the period.

So, the peak pulse power P_{peak} is the maximum optical power that can be maintained for a certain limited period of time (i.e. optical power per pulse). The peak power P_{peak} can be determined through the ratio of average power P_{avg} to the product of the pulse repetition rate f_{rep} by the pulse width τ as shown in the equation:

$$P_{peak} = \frac{P_{avg}}{f_{rep}\,\tau} = \frac{P_{avg}}{\tau}\,\Delta t\ , \tag{3}$$

where τ is a pulse duration [25]. The pulse duration τ (or in other words, pulse width/pulse length) is a measure of the time between the beginning and end of a pulse, usually based on the half-maximum of the full width (FWHM) of the pulse shape. The value of the pulse duration τ can range from several tens of picoseconds to arbitrarily high values.

The main purpose of using parameters of the pulse energy E and pulse duration τ is estimation the peak power P_{peak} of the pulse sequences.

The generation of optical pulses can be realized using a continuous emitting laser light source and a fast modulator that transmits light for a certain period of time (quasi-continuous regime). However, this method is ineffective due to the loss of most of the light on the modulator; moreover, the pulse duration is limited by the response speed of the modulator and the peak power does not exceed the average power. Optical pulses having significantly higher energies and significantly shorter pulse durations can be generated in lasers designed to operate in pulsed regime. The most common methods to generate short and ultrashort pulses are Q-switched and mode-locked methods that are discussed in detail in the following subsections [26].

3.2.1 Q-switching

A Q-switched method is of generating energetic short laser pulses, using modulation of intracavity losses and, therefore, Q-factor of a laser resonator. This method is mainly used for the generation of nanosecond pulses of high energy (with energies in millijoules and more) and peak power for solid-state bulk lasers. The main idea of the Q-switched method is introducing high intracavity losses (intracavity shutter is closed) preventing the laser from emitting. Due to this, the power is not spent on radiation, but accumulates; thereby it is possible to obtain a high level of population inversion of upper energy levels of the active medium. Opening the intracavity shutter results in sudden losses reduction so that the laser radiation emits. All stored energy is realized in the form of a short, powerful pulse [10].

The Q-switch method can be implemented using two mirrors so that one of the mirrors is made movable (rotating). At moments when the rotating mirror is not parallel to the fixed mirror, the quality factor of the resonator is low and there is no radiation; when the mirrors

become exactly parallel to each other, the quality factor of the resonator increases sharply, and the laser begins to emit. Second approach for Q-switch technique is an acousto-optic modulator. A periodic RF signal is applied to the modulator enabling on/off conditions [26], [27].

A simplified diagram of the implementation of an active Q-switched method is shown in the Figure 8. The Q-switched shutter (rotating mirrors or acousto-optic modulator) is activated at time t = 0, as a result of which a pulse is formed after the arrival of the electric trigger signal. Thus, power begins to grow exponentially, as shown in Figure 8.

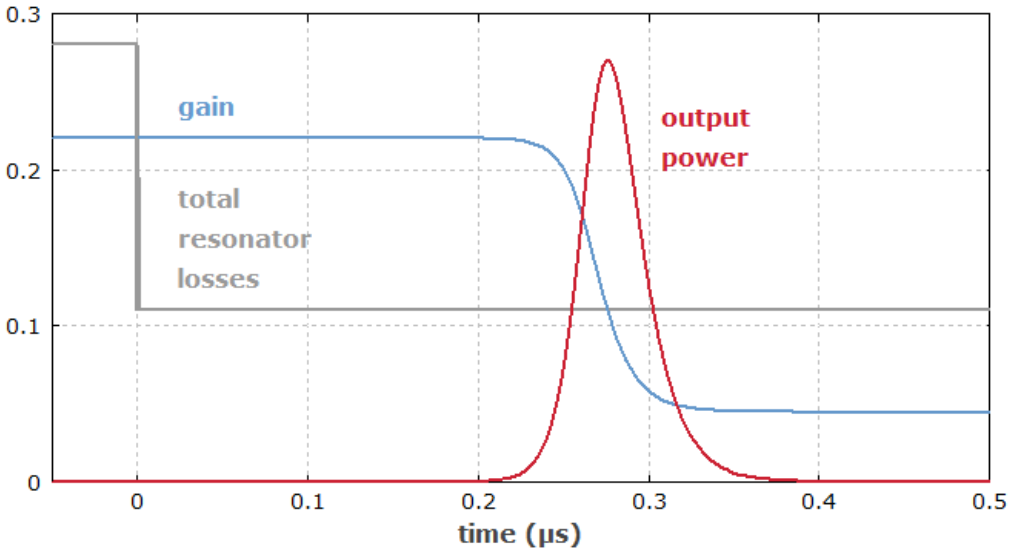

Fig. 8. A simplified laser gain and loss scheme using a Q-switched method [10].

3.2.2 Mode-lock

The mode-locked method is used for generation of ultrashort light pulses [28]. The mode-locking is a technique in which is possible to synchronize the phases of various longitudinal modes in a laser (Fig. 9), thereby obtaining ultrashort pulses in the range of pico- or femtoseconds. The interference between these modes causes the laser radiation to be a sequence of pulses [10].

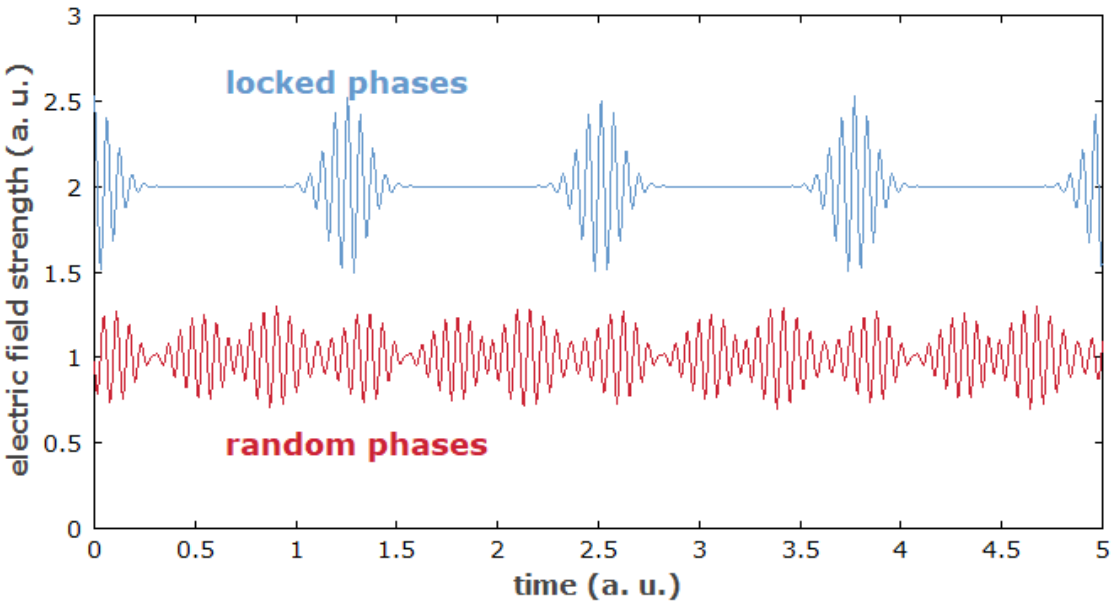

Fig. 9. Demonstration of the intracavity field in the laser (blue line is mode-locked method and red line is temporal evolution with random phases) [10]

There is active mode synchronization using a modulator device involving periodically modulating cavity losses or phase changes in both directions a fast acousto-optic or an electro-optical modulator [10]. Active mode-locking can lead to the generation of ultrashort pulses, usually with a duration of picosecond pulses [28].

There is also passive mode synchronization using a saturable absorber, which allows the generation of significantly shorter, femtosecond, pulses. The reason is that a saturable absorber, which is driven by short pulses, can modulate resonator losses much faster than an externally driven modulator [10], [28].

Using the mode-locked seed lasers and high-power amplifiers, the amplification of an ultrashort laser pulse to a petawatt level is realized [29]. This method of amplification is called chirped pulse amplification (CPA), in which the laser pulse is initially stretched in time, then amplified, and then compressed again delivering ultra-short high-intense pulses at the output.

Nowadays, high-intense pulsed solid-state lasers system have demonstrated dramatic progress and become attractive for many laser-driven applications. Often in such applications the ultra-short high-power beam should be safely delivered over several meters to the workpiece. The most convenient approach for delivering pulsed light over long distances is an optical fiber, which will be discussed in detail in the next section.

4. OPTICAL FIBER

An optical fiber is a convenient tool for beam delivery over long distance due to intrinsic mechanism of the light confinement. This feature of the optical fiber is applicable equally for low and high-power light. However, a special fiber structure is required to overcome the challenges related to propagation of high-power density beam in the confinement conditions. This chapter describes the specific characteristics and light propagation mechanisms in optical fibers. It includes the comparison and differences between single-mode, multimode and large mode area fibers. The latter is specifically designed for high-density beam transmission.

4.1 Mechanism of light confinement

The conventional optical fibers have a core with a refractive index that exceeds the refractive index of the surrounding medium, the cladding [30]. The simplest case is a fiber with a step-index profile where the refractive index is constant inside the core and inside the cladding (Fig. 10 (a)) [10]. Another approach is graded-index optical fibers (Fig. 10 (b)) [31]. Unlike standard optical fibers having a constant refractive index profile of the core material, graded-index optical fibers have a refractive index that gradually decreases from the center to the cladding. Due to changes in the speed of light propagation, the propagation delay of different light modes is compensated. As a result, such optical fiber has many times less dispersion, and, consequently a large pass band. The main disadvantage of gradient optical fibers limiting their use is the high price and complexity of production. The step-index and graded-index profiles are shown in the Figure 10 below [32].

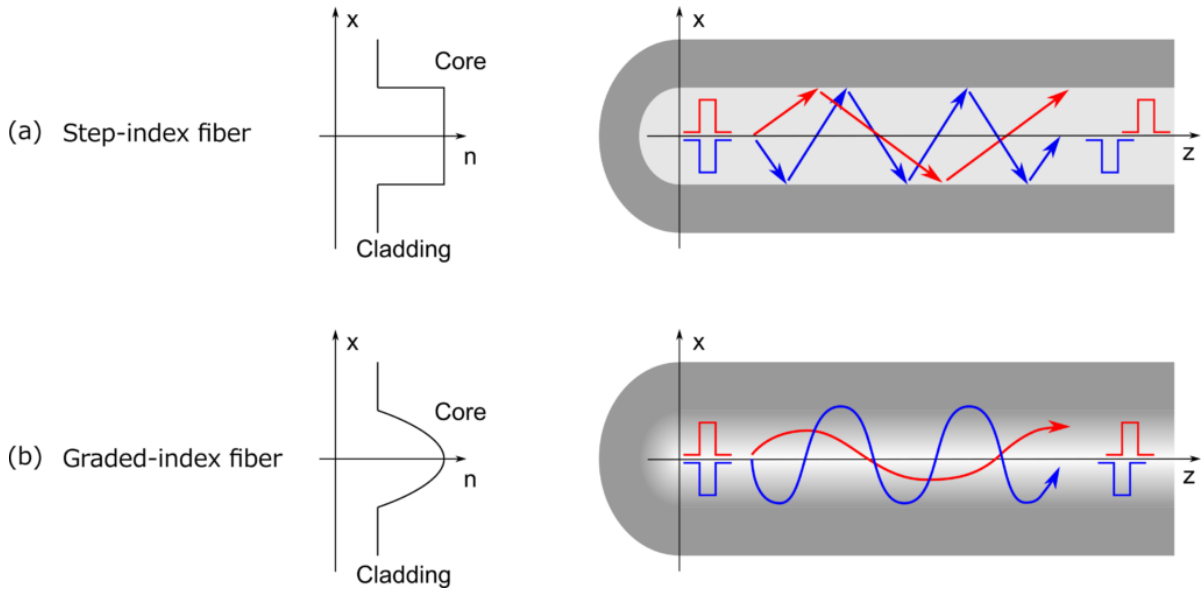

Fig. 10. Light guidance in (a) step-index and (b) graded-index optical fiber [32].

Light propagates directly through the core of the conventional fiber due to the phenomenon of total internal reflection (TIR) [33]. Because of the difference in the refractive indices of the core n_1 and cladding n_2, light waves are propagating in the core at an angle not exceeding a critical value and undergo total internal reflection (TIR) from the optical cladding (Fig. 11). This follows from Snell's law of refraction [34], which states that total internal reflection (TIR) occurs at any angle of incidence greater than the critical angle θ_c, and this can only happen when the second medium has a refractive index n_2 less than the first n_1.

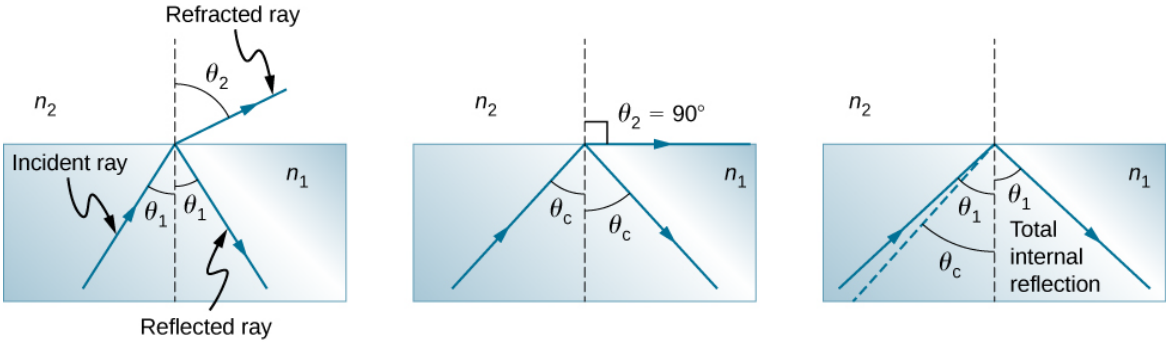

Fig. 11. Refraction of light at the interface between the fiber core and the cladding, including total internal reflection [33].

The following relation determines the critical angle θ_c:

$$\theta_c = sin^{-1}\frac{n_1}{n_2}, \quad (4)$$

where n_1 and n_2 are refractive indices of the fiber core and the cladding, correspondingly [32].

By repeated reflections from the cladding, the waves propagate along the optical fiber. Light waves that propagate in a fiber over considerable distances are called spatial modes of optical radiation. The concept of a mode is described mathematically using the Maxwell equations for electromagnetic waves; however, in the case of optical radiation, it is convenient to understand modes as the propagation paths of allowed light waves [35].

Currently, optical fibers are designed to support either one propagating mode or several modes. Such fibers are called single-mode and multimode, respectively. A more detailed description of such fibers is presented in the next section 4.2.

4.2 Single-mode and multimode propagation

An optical fiber can support one or more controlled modes in which the intensity distributions are located inside or directly around the fiber core, but nevertheless some of the intensity can pass into the fiber cladding. Examples of possible mode patterns propagating in the optical fiber are shown in the Figure 12 [36].

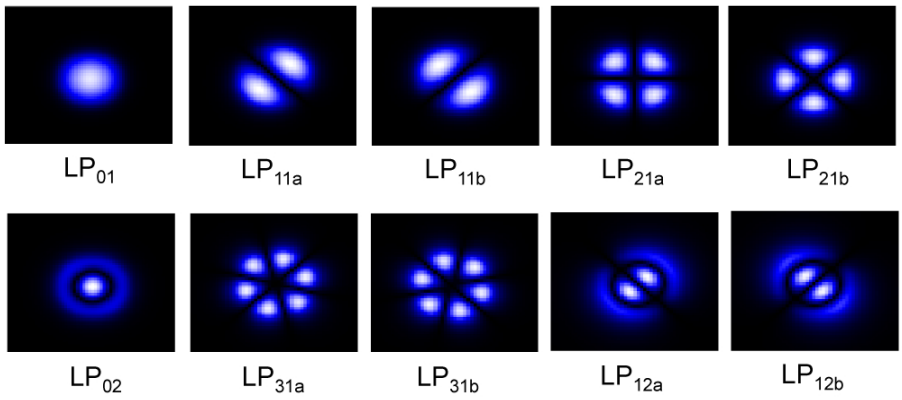

Fig. 12. Examples of the spatial intensity patterns of modes in an optical fiber [36].

Two types of optical fiber are distinguished: multimode and single-mode optical fibers [37]. The difference between them is in different ways of passing by the light flux inside the fiber. In a single-mode optical fiber, the beam travels as one path (LP_{01} mode, Figure 12), so the light rays reach the receiver at the same time. In such a fiber, the signal is lost only slightly, so it can be easily transmitted over long distances without beam uniformity degradation. In a multimode optical fiber, light rays have a significant scattering, as shown in Figure 13, which leads to a strong distortion of beam at the end and formation of complex spatial pattern (Figure 12) [38].

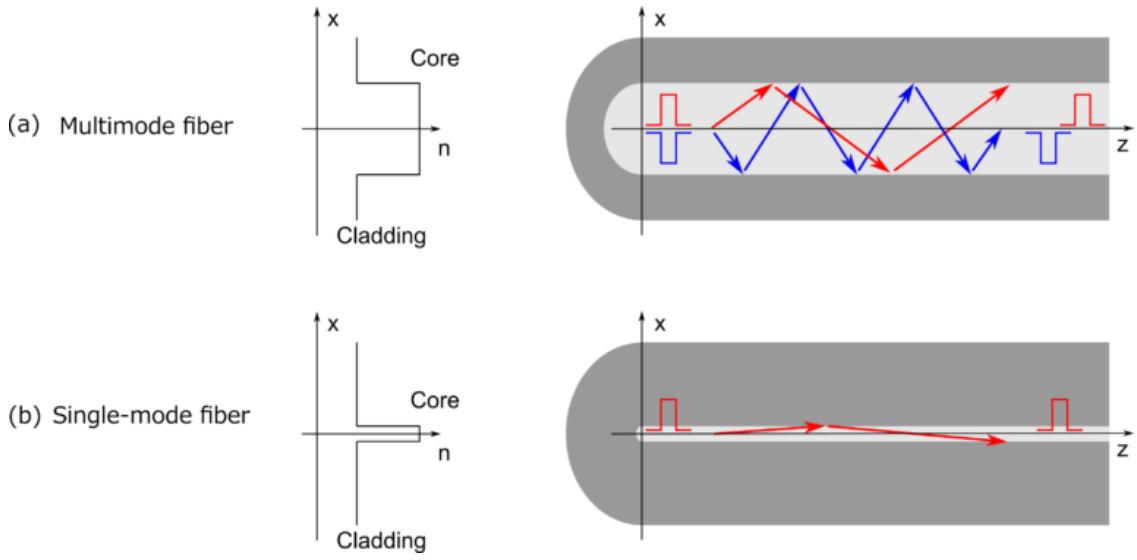

Fig. 13. Schematic representation of the (a) multimode and (b) single-mode optical fiber [32].

Important differences between single-mode and multimode optical fibers are specified as follow [10]:

• Single-mode fibers contain a core of mainly small size, the diameter of which is only a few micrometers. The mode radius in a single-mode fiber is approximately 5 μm. Such fibers can direct only a single spatial mode, in which in most cases the profile is approximately Gaussian as presented in the Figure 14.

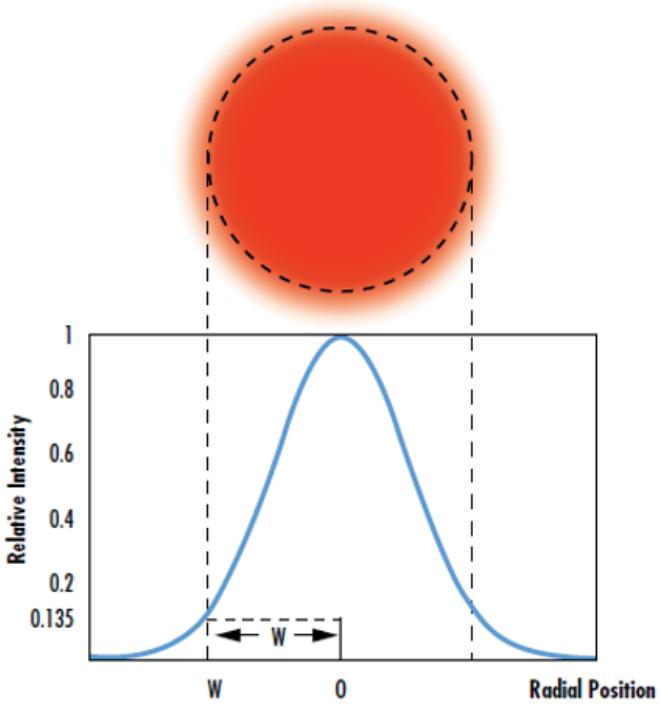

Fig. 14. Schematic image of a Gaussian shape mode-profile distribution [39].

When the conditions for introducing a light beam change (i.e. beam divergence and MFD), the power that is launched into the guided mode also changes, while the spatial distribution of light emerging from the optical fiber is fixed. To efficiently launch light into a single-mode fiber, a laser source with good beam quality is needed, and the input beam must be collimated to ensure accurate alignment of the focusing optics to achieve mode matching.

• Multimode fibers have a sufficiently large core, the diameter of which is typically more than 50 μm, as well as a large difference between the refractive indices of the core and cladding, which makes it possible to maintain several modes with different intensity distributions. In the case of multimode fibers, the spatial profile of the light beam that leaves the fiber core depends on the conditions for launching the light beam, which determine the power distribution between the spatial modes.

The difference in refractive indices between the core and the cladding of the optical fiber determines the numerical aperture (NA) of the fiber, which is considered in the next section.

4.3 Parameters of optical fibers

Numerical aperture (NA)

An optical fiber is characterized by the radius of the core *a* and the difference in refractive indices between the core and the cladding. Typical core radius values are several microns for single-mode fibers and tens of microns or more for multimode fibers [10]. The numerical aperture (NA) of an optical fiber is a measure of angular perception for incoming light. Qualitatively, it is a measure of the ability of a fiber to collect light. It also indicates how easy it is to connect the light into a fiber. NA is determined on the basis of geometric considerations and, therefore, the numerical aperture is a theoretical parameter that can be calculated from an optical fiber design. It cannot be measured directly, but there are exceptions as limiting cases with large apertures and insignificant diffraction effects [40].

For a fiber with a step-index, it is possible to define the numerical aperture (NA) as a difference in refractive indices between the core n_{core} and the cladding $n_{cladding}$ using the equation [10]:

$$NA = \frac{1}{n_o}\sqrt{{n_{core}}^2 - {n_{cladding}}^2}\,, \tag{5}$$

where n_0 is the refractive index of the medium surrounding the fiber, which in the case of air is close to 1 [10].

Rays that extend beyond the angle specified by the numerical aperture (NA) fiber are the radiation modes of the fiber. A higher core index with respect to the cladding means a larger numerical aperture (NA). However, an increase in numerical aperture (NA) leads to higher scattering losses at higher dopant concentrations. The numerical aperture (NA) of fibers can be determined by measuring the angle of divergence of the light cone that it emits when all its modes are excited.

The efficiency of light launching into the fiber, losses in microbends and the number of propagating modes are related to numerical aperture (NA). Fibers having an aperture greater than 0.2 are called high aperture fiber, and less than 0.2 are called low aperture fiber. High aperture fibers have a relatively low input loss, are insensitive to bending, but have a high propagation loss. They are used to transmit signals over short distances. Low aperture fibers are widely used due to stronger light confinement effect.

V-number

A number of propagating modes is defined by the *V*-number parameter:

$$V = \frac{2\pi}{\lambda} aNA = \frac{2\pi}{\lambda} a \sqrt{n_{core}^2 - n_{cladding}^2} \ , \tag{6}$$

which is called the normalized frequency [10]. Single-mode propagation in a fiber is achieved when the *V*-number is below ≈ 2.405. Multimode fibers can have much higher *V* values. The number of modes then scales with V^2. As it can be seen from the equation 6, low NA results in low *V*-number. By increasing the core radius and simultaneously decreasing NA *V*-number can remain close to 2.405 resulting in the single-mode propagation in the fiber even with large core.

Mode radius

For single-mode fibers with a step-index profile, the mode radius *w* can be calculated from the radius of the core of the optical fiber *a* and a normalized frequency *V* using the Marcuse equation [10]:

$$\frac{w}{a} = 0.65 + \frac{1.619}{V^{3\backslash 2}} + \frac{2.879}{V^6}. \quad (7)$$

It can be seen from the equation (7) that the mode radius *w* becomes smaller for higher frequencies with higher *V*-number [10]. Typical mode radius for single-mode fiber is around 3 μm. The small mode radius supports good quality beam propagation at long distance without intermodal interference. However, a conventional single-mode fiber is not suitable for intense light propagation because high-power density is concentrated in a small cross section of the fiber core, which will lead to the appearance of nonlinear effects. Nonlinear effects are discussed in detail in section 5.

A decrease in peak power density is possible when using an optical fiber with a large core size. As the core size increases, the numerical aperture (NA) must be reduced accordingly for maintaining a single-mode propagation. This is a challenging task and several practical solutions have been invented to surpass the problem. They are described in the next section.

4.4 Large effective mode area fibers (LMA fibers)

Large mode area fibers (LMA) are a growing field of research, in particular due to the increase in available high-power light-emitting laser sources, and the need for fiber-optic components to deliver a high-quality optical beam [41]. The main objective is to develop fibers that in practice support only one core guided mode with minimal bending loss. In this section, we will consider the currently available fiber options with a large mode area (LMA) [10].

Currently, the output power of solid-state lasers reaches tens of kilowatts of average power. At such high intensities of the output radiation in conventional optical fibers, the threshold for the excitation of nonlinear effects and even destruction is easily reached, which makes them unsuitable for applications in areas where a high output power of optical radiation is required. In this regard, the possibility of developing and studying fibers with a large mode area for applications related to high-power solid-state lasers and powerful amplifiers is currently being widely studied. An increase in the effective mode area leads to a decrease in the power density of optical radiation propagating through the fiber, due to which nonlinear effects and material destruction have larger threshold in such fibers. An

important parameter for such fibers is the high quality of the output beam and low sensitivity to bending. While conventional single-mode optical fibers have an effective mode area below 100 μm^2, fibers with a large mode area reach hundreds or even thousands of μm^2 (Fig. 15) [41].

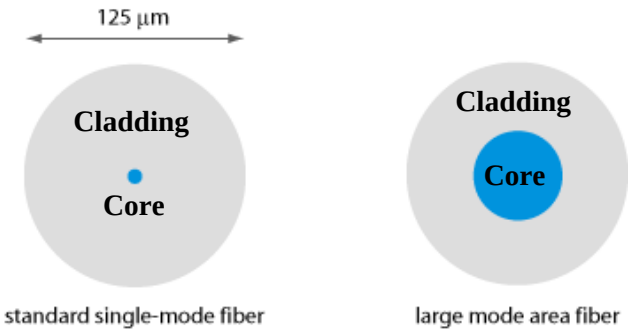

Fig. 15. Comparison of bare (uncoated) fibers with a standard core size, 8 μm diameter and a large core, 50 μm diameter [10].

A possible approach to design large mode regions is to reduce the numerical aperture (NA), i.e. to reduce the difference in refractive indices between the core n_{core} and the cladding $n_{cladding}$, for a fiber design with a step index, as shown in Figure 16 [10].

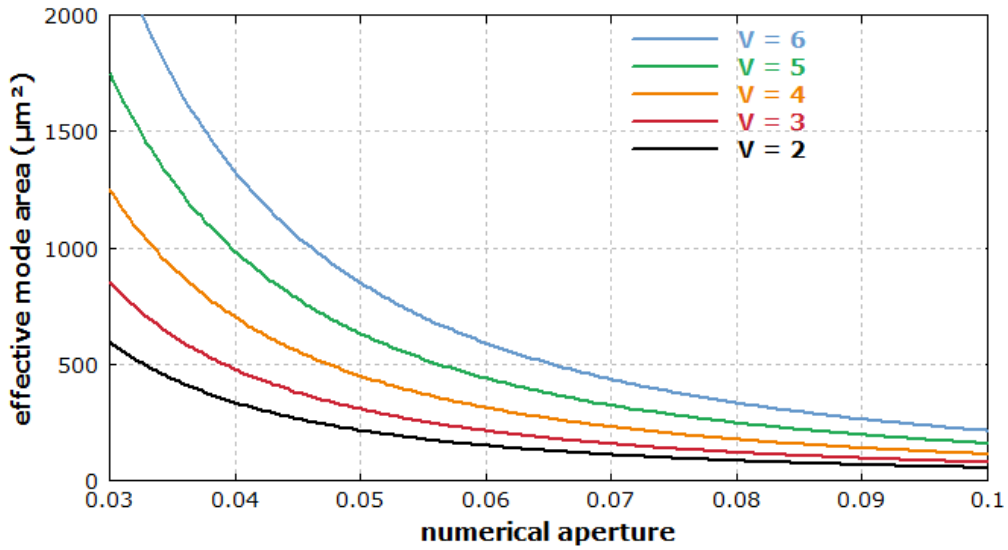

Fig. 16. The dependence of the effective mode area of the fiber with the step-index from the numerical aperture for various values of *V*-number [10].

However, with a large decrease in the numerical aperture (NA), some serious limitations appear: a light guidance can be weakened, and significant losses can occur due to small fiber defects or fiber bending. Therefore, the numerical aperture (NA) of the optical fiber should usually not be less than about 0.06 [10].

The possible compromise can be found in the fibers supporting the propagation of a few modes, however, it should be designed so to introduce low loss for fundamental mode and higher losses for higher-order modes. This approach simplifies the maintenance of reliable single-mode propagation in a multimode fiber. The list of the most important technical solutions invented for this approach is presented below [10].

• *Fiber bending*. Fiber bending, a schematic representation of which is shown in the Figure 17, helps to introduce different coupling conditions for fundamental mode and high order modes.

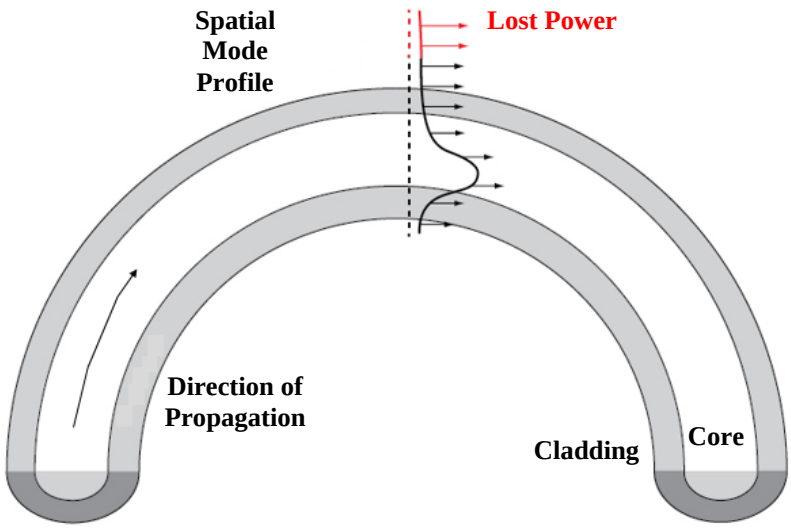

Fig. 17. Presentation of a technical solution for decrease of undesired mode coupling by fiber bending [25].

• *An optical fibers with a chiral-coupled core.* This type of fiber has two cores, the first is a straight center, where a light beam propagates; the second is a spiral, i.e. spirally wound around the central core, as shown in Figure 18.

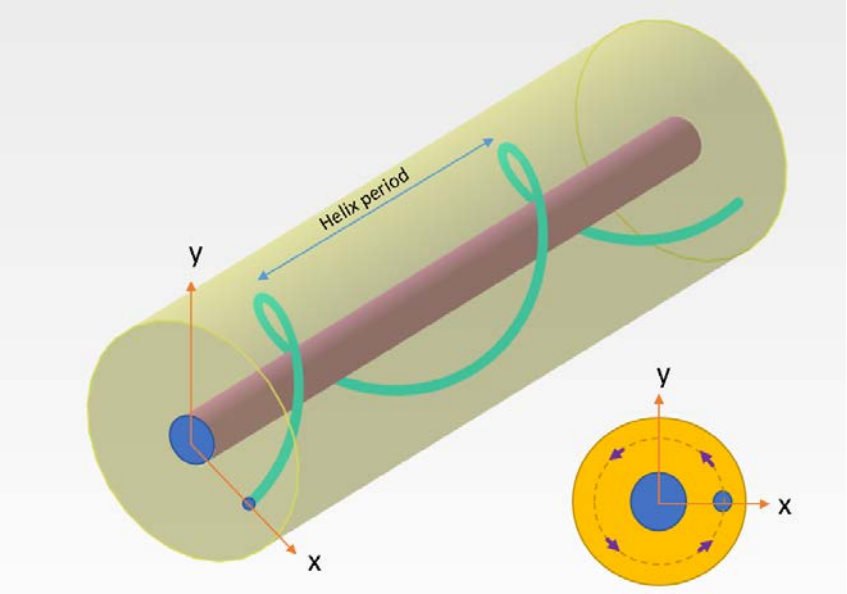

Fig. 18. An example of an optical fiber with a chiral-coupled core that consists of a straight central core and a side core with a helical shape [42].

This fiber design provides selective coupling of the higher-order modes of the central core into the spiral core, while the fundamental mode remains almost unchanged. The principle of such selective coupling is the effect of helicity on the propagation constant so that in a certain wavelength range, phase matching is realized only for coupling of higher-order modes, but not for the fundamental mode. Thus, the fundamental mode propagates through the straight core, and higher-order modes go to the spiral core [10], [42].

• *Optical fibers with leakage channels*. In this fiber design, the core is surrounded by a set of large holes, as a result of which leakage of propagating modes is realized strictly according to the selective principle: all modes with a higher-order have significant propagation losses, while the fundamental mode remains almost unchanged [10], [43]. The design of the optical fiber with leakage channels is shown in Figure 19 (a).

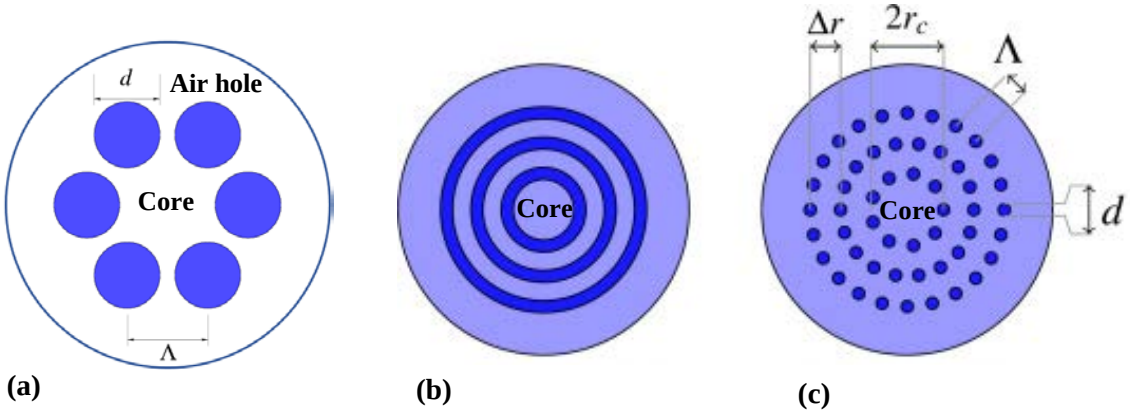

Fig. 19. Schematic cross-sections of (a) all-glass fibers with leakage channels [43], (b) a Bragg fiber and (c) a pixelated Bragg fiber [44].

• *Pixelated Bragg fibers*. The design of pixelated Bragg fibers is a modified version of the Bragg fibers, that is, fibers with a sequence of continuous rings with a high refractive index (Fig. 19 (b)). In pixelated fibers, discontinuous (pixelated) rings in the shape of round-rod with a high index replace these continuous high-index rings (Fig. 19 (c)), so that propagation losses become high for higher order modes, while losses remain low for the fundamental mode. As a result, a limited number of cladding modes will create an area without coupling where only the fundamental modes can exist, which will introduce a real Photonic Bandgap (PBG) control mechanism [10], [44].

The fiber designs having a large mode area can reach an effective mode region of a size of several thousand μm^2. These fibers are highly valuable for intense light delivery, however, they exhibits less stable single-mode propagation and often can only allow very slight bending.

The current state-of-the art in terms of delivery fiber is the microstructured fiber with intrinsic mechanism of leaking channels for higher-order modes. The details of mode propagation in these fibers are described in the next section.

4.5 Microstructured optical fibers

The mode discrimination during propagation can be realized using special fibers, which are called photonic crystal fibers (or index-guided fibers) [45] and photonic bandgap fibers (PBG fibers) [10]. Their recent invention for single-mode propagation has created great potential for transmitting high power laser pulses. Such fibers have complex cross-sectional geometry, including air holes in the cross-section the silica glass. The distinctive feature of these fibers is the mode confinement obtained by manipulating the waveguide structure rather than its refractive index [46].

A photonic crystal fiber (also called microstructured optical fiber or “holey” fiber), a schematic illustration of the cross section of which is shown in Figure 20 (a), is constructed from the same material like conventional fiber, usually silica, and the light guide is realized by the presence of air holes in the area that surrounds the solid core [47]. Those very small and closely spaced air holes extend along the entire length of the fiber. Holes can be arranged regularly in two-dimensional arrays, but there is also a non-periodic pattern of holes. In such a “holey” fiber, the region with air holes has a lower average refractive index than the core of the fiber. In this case, the guiding mechanism is the standard total internal reflection (TIR), as in optical fibers with a step refractive index [10].

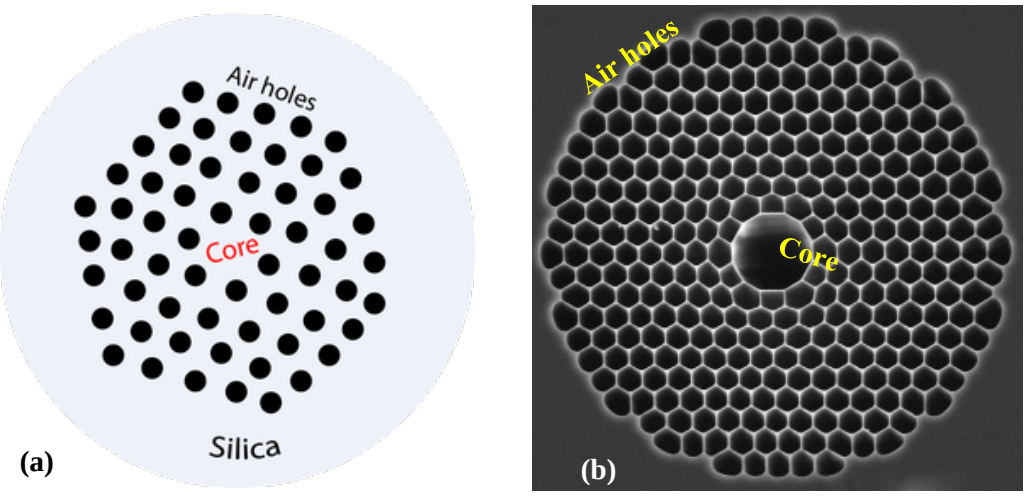

Fig. 20. Schematic illustration of the cross section of (a) a photonic crystal fiber [48] and (b) a photonic bandgap fiber [10].

In a photonic band gap fiber (PBG fibers) the guiding light is obtained by the constructive intervention of scattered light. A schematic illustration of the cross section of a photonic band gap fiber is shown in Figure 20 (b). In fact, the design of such a fiber implements photonic bandgap control using a kind of two-dimensional Bragg mirror (Bragg reflector) surrounding the core of the fiber. In this case, the guide is highly dependent on the wavelength due to the Bragg reflection. Therefore, such guiding mechanism usually works only in limited region of wavelengths. The refractive index of the core in such fiber may be lower than the index of the cladding. Moreover, the core can even be hollow, so that the refractive index of the core is equal to the air (approximately 1) [10].

Photonic crystal fibers and photonic band gap fibers have a significant advantage, a very small nonlinearity. This makes them promising for transmission of high-power laser radiation. Both designs can have very large mode area of the optical fiber core when focusing on only single-mode propagation for limited diffraction output, and thus they are suitable for very high output powers having excellent beam quality. On the other hand, such fibers also have a number of disadvantages: production difficulties due to their tight manufacturing tolerances, limited bandwidth for low-loss transmission, and relatively high propagation losses [10].

5. NONLINEAR EFFECTS IN OPTICAL FIBERS

When a high-power pulse is transmitted through optical fibers, the light-matter interaction results in appearance of nonlinear effects, which in their turn lead to the pulse and beam distortions. This chapter will reveal the physical mechanism of the light-glass interaction and nonlinear effects arising in the fiber such as Stimulated Raman scattering, the Kerr effect and Stimulated Brillouin scattering.

5.1 Nonlinear effects in optical fibers

In an optical fiber, the light beam propagates over long distances along the fiber and it is limited by the transverse region of the fiber. That is why nonlinear effects often have significant influence. This is especially important for the case when fibers are used to transmit ultrashort high-power laser pulses. The essence of nonlinear effects is that a propagating light beam causes a change in the characteristics of the fiber through which it propagates, and this, in turn, already leads to a very significant change in the propagation conditions of the light beam itself [49].

Nonlinear phenomena in an optical fiber are caused by the nonlinear response of a fiber material to an increase of the light flux intensity. As a result, the optical characteristics of the fiber medium (such as an electronic polarizability, a refractive index, an absorption coefficient) become functions of the electric field of the light wave, so that the polarization of the medium begins to depend nonlinearly on the field strength [49].

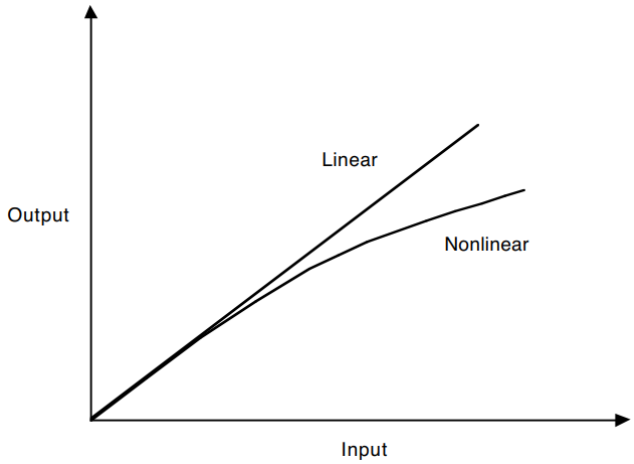

Fig. 21. Nonlinearity of power during the propagation of a laser pulse along the optical fiber. The horizontal axis is the input power; the vertical axis is the output power [49].

The polarizability of the dielectric *P* is proportional to the field strength *E* only in weak electric fields. In strong fields, the polarizability *P* depends on the field strength *E* nonlinearly (Fig. 21). In fact, the reason for the nonlinearity is the inharmonic motion of bound electrons under the influence of an applied field. Because of this inharmonic motion, the total polarization *P* that is induced by electric dipoles is not linear, but satisfies a more general equation, as:

$$P = \varepsilon_0 \times \chi^{(1)} \times E + \varepsilon_0 \times \chi^{(2)} \times E^2 + \varepsilon_0 \times \chi^{(3)} \times E^3 + \cdots , \qquad (8)$$

where ε_0 is the permittivity of vacuum and $\chi^{(k)}$ (k = 1, 2,...) is k^{th} - order nonlinear susceptibility [49].

The first nonlinear term $\chi^{(2)} \times E^2$ in isotropic materials and crystals with a center of symmetry is zero. All nonlinear effects appearing in quartz optical fibers are associated with third-order nonlinearity $\chi^{(3)} \times E^3$. Silica has a low nonlinear susceptibility $\chi^{(3)}$, but with a large optical fiber length, nonlinear effects accumulate and become pronounced. These effects with third-order nonlinearity $\chi^{(3)}$ can be divided into two classes. They differ in whether the induced polarization oscillates with the frequency ω of the incident field or not. The first class includes the so-called self-induced effects, which are described using a

nonlinear refractive index (optical Kerr effect). The second class includes stimulated Raman scattering (SRS) and Brillouin scattering (SBS) [49].

The next section discusses in detail the main nonlinear effects that affect the characteristics of optical fiber systems, such as the Kerr effect [10], stimulated Raman scattering [50] and Brillouin scattering [50].

5.2 The Kerr effect

The Kerr effect is an electro-optical feature that includes both the orientation of the molecules under the influence of an electric field and the polarizability anisotropy, which is then observed in the medium. In other words, the Kerr effect is the phenomenon of a change in the refractive index of an optical material under the influence of an applied constant or alternating electric field. Isotropic materials that have refractive indices independent of the direction in the medium become anisotropic, in other words, they have different refractive indices in different directions when they are exposed to an electric field. A partial molecular orientation and directional structure is superimposed in this way that give rise to the observed effect [51].

The Kerr effect occurs when intense light beam propagates in the optical fiber. The physical origin of the Kerr effect is a nonlinear polarization generated in a fiber medium that itself changes the properties of light propagation. Non-linear response can be described as a change in the refractive index. In particular, the difference in refractive indices for the high-intensity light beam itself varies in accordance with the equation [10]:

$$\Delta n = K \times E^2 , \tag{9}$$

where K is the Kerr coefficient and E is the electric field strength. Refractive index difference is proportional to the squared of the electric field strength.

At extremely high optical intensities, there can be no further increasing in the refractive index in proportion to the intensity, but saturation and a significant decreasing in the value

of the refractive index. This is due to the multiphoton ionization effect, which leads to induced losses along the beam propagation.

5.3 Stimulated Raman scattering

The nonlinear response of a silica glass medium in optical fiber to the optical intensity of light beam propagating through a glass core over a long distance is very fast, but not instantaneous. Particularly, the reason for the non-instantaneous response is crystal lattice vibrations. In the case when the crystal lattice vibrations are associated with optical phonons, the effect is called Raman scattering [10].

When a light beam propagates in the silica glass core of an optical fiber, it interacts with the fiber material (silica glass) resulting in the inelastic scattering of photons by fiber matter (silica glass), which is accompanied by a noticeable change in the radiation frequency. In Raman scattering, photons are scattered due to vibrational and rotational transitions in bonds between neighboring atoms. This includes vibrational energy received by a molecule from incident photons [50].

From the point of view of classical theory the electric field of light induces an alternating dipole moment of the molecule in the silica glass material, which oscillates (vibrates) with the frequency of the incident light, and changes in the dipole moment in turn lead to the emission of radiation from the molecule in all directions. In the classical model, it is assumed that a silica glass substance contains charges that can be separated, but some forces acting along with Coulomb attraction hold them together. The formation of a wave at the interface with the matter causes an oscillatory separation of these charges, and as a consequence, an oscillating electric dipole appears radiating at the oscillation frequency. This radiation is also scattering [10].

From the point of view of quantum theory, the origin of this effect is most conveniently explained in the framework of the quantum theory of radiation. According to it, radiation of frequency v is considered as a flux of photons with energy hv, where h is the Planck constant. In collisions of the light beam with molecules of the silica glass material, photons scatter. In the case of elastic scattering, they will deviate from the direction of their motion without

changing their energy (Rayleigh scattering). But it may also be that in a collision an energy exchange takes place between a photon and a molecule. In this case, the molecule can either gain or lose a part of its energy in accordance with the quantization rules. Its energy can change by ΔE, which corresponds to the energy difference between its two allowed states. In other words, ΔE must be equal to the change in the vibrational and/or rotational energies of the molecule. A schematic representation of the Raman scattering and its comparison with elastic Rayleigh scattering is presented in the Figure 22 [10].

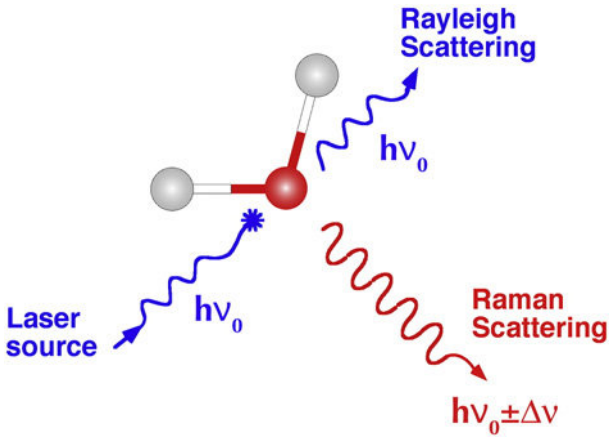

Fig. 22. A simple layout of light scattering processes with a simple molecule: Rayleigh scattering (blue color) and Raman scattering (red color) [52].

If a molecule gains energy ΔE, then after scattering the photon will have energy $(h\nu - \Delta E)$ and, accordingly, the radiation frequency $(\nu - \Delta E/h)$. And if the molecule loses energy ΔE, the radiation scattering frequency will be equal to $(\nu + \Delta E/h)$. Radiation scattered with a frequency lower than that of the incident light is called Stokes radiation, and radiation with a higher frequency is called anti-Stokes, as shown in the Figure 23 [50].

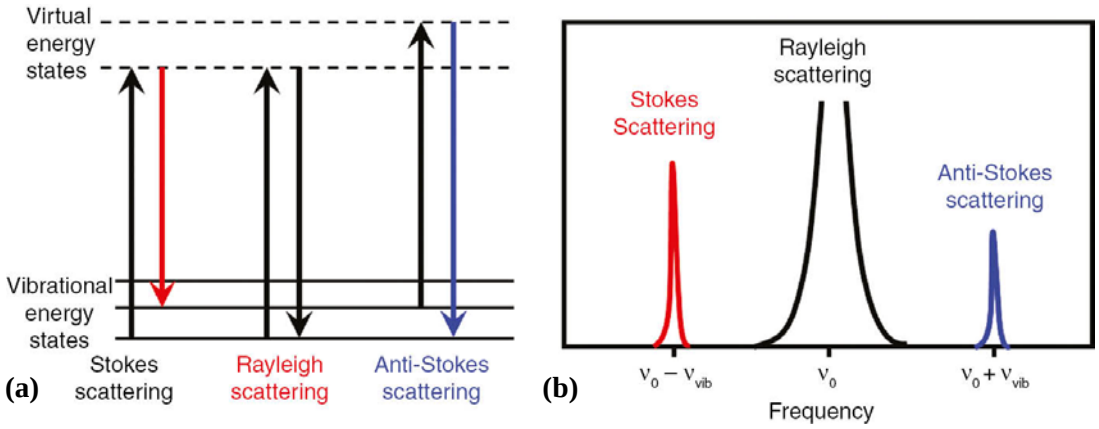

Fig. 23. Schematic representations of (a) Rayleigh and Raman scattering and (b) illustrative diagram of resulting Raman spectrum [52].

Thereby, the Raman scattering effect in the optical fiber is manifested in the fact that the light beam is scattered due to nonlinear interaction with silica glass material and shifted to the region of longer waves. The effect can occur in a wide optical spectrum (approximately 7 THz), for example, of an ultrashort optical pulse, effectively shifting the envelope of the pulse spectrum in the direction of longer wavelength by a value of the order of 10...13 THz. Raman scattering depends on the frequency of the incident light; it is more pronounced at higher frequencies compared to low frequencies [10].

The Raman scattering effect can be characterized by the value of the threshold power, which can be determined from the equation:

$$P_t = \frac{16\, A_{eff}}{g_R\, L_{eff}}, \tag{10}$$

where A_{eff} is the effective core area of the optical fiber, g_R is the Raman gain and L_{eff} is the effective length of the optical fiber, defined as follow:

$$L_{eff} = \frac{1}{\alpha}(1 - exp(-\alpha L)), \tag{11}$$

where α is the constant attenuation coefficient and L is the length of the optical fiber [52].

When transmitting a high-power laser pulse through a long delivery fiber, Raman scattering is harmful: Raman scattering can transfer most of the pulse energy to the wavelength range where laser amplification does not occur. As a result, this effect causes losses and pulse distortions. Hereby, the Raman scattering imposes significant restrictions on the maximum transmitted radiation power propagating through a delivery fiber.

5.4 Stimulated - Brillouin scattering

Stimulated Brillouin scattering is the scattering of optical radiation in a fiber material due to the interaction of a light beam with inhomogeneities of the medium. As inhomogeneities can be thermal fluctuations of the medium. A relatively strong interaction between the particles of the condensed matter of the fiber (it binds them into an ordered spatial lattice) leads to the fact that these particles cannot move independently. Any of their excitation propagates in the medium in the form of an acoustic wave. At any temperature other than absolute zero, the particles are in thermal motion. As a result, elastic waves of different frequencies propagate in different directions in the medium. An example of the propagation of an elastic wave is shown in the Figure 24 [50].

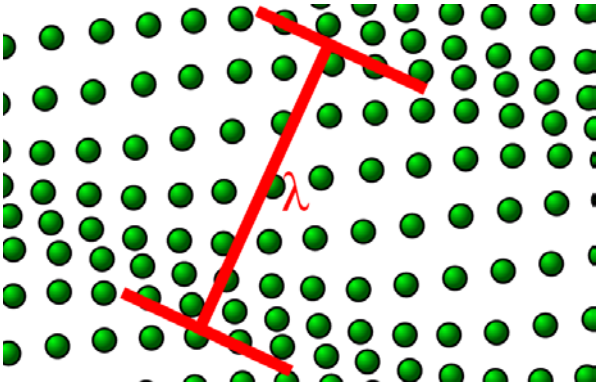

Fig. 24. Presentation of the wave propagating through a crystal lattice [53].

Thus, Brillouin scattering sets an upper limit on the level of maximum achievable optical power, which can be transmitted through an optical fiber. When the threshold level of optical power is exceeded, an acoustic wave appears in the optical fiber, under the influence of which the value of the refractive index changes. Changes in the refractive index cause light scattering, leading to additional generation of acoustic waves, as a result of which the useful

transmitted optical power is attenuated. The expression for the threshold power can be represented as:

$$P_t = \frac{21\, A_{eff}}{g_B\, L_{eff}} \times \left(1 + \frac{\Delta\nu_{LS}}{\Delta\nu_B}\right), \tag{12}$$

where g_B is the Brillouin gain [50].

The Brillouin scattering effect can occur due to the propagation of a narrow laser spectrum only: the stimulated emission spectrum is no more than 60 MHz and it is shifted to the long-wavelength side by 10 ... 11 GHz. Thus, in the case of a wide spectrum (corresponding to ultra-short pulses) Brillouin scattering does not occur [10].

6. EXPERIMENTAL PART

This chapter presents the study of a novel W-type large-mode-area delivery fiber developed for transmission of ultrashort intense pulses over several meters' length. The experimental investigation includes the measurements of bending losses, output beam quality as well as design of free-space light coupling system.

6.1 Large mode area W-type delivery optical fiber with a single-mode propagation

In recent years, there has been a significant increase in the power of solid-state lasers, which in turn requires spectacular performance of the main key component for transmitting high-power radiation over long distances, a delivery fiber. At the moment, the output power of solid-state lasers reaches tens of kilowatts. At high intensities of the output radiation in conventional optical fibers, the threshold for the excitation of nonlinear effects and even destruction is easily reached, which makes them unsuitable for applications in areas where a high-power output optical radiation is required.

In this regard, the possibility to develop and to study delivery optical fibers with a large mode area for applications related to high-power solid-state lasers and high-power amplifiers is currently being widely studied. An increase in the effective mode area leads to a decrease in the power density of the optical radiation propagating through the fiber, as a result the thresholds for nonlinear effects increase. Due to potential applications and practical issues the most important parameters for such fibers are the high quality of the output beam and low sensitivity to bending due to the strong localization of the field in the core [10].

This Master thesis presents a detailed experimental study of the properties and basic characteristics of almost single-mode optical fibers with a large mode area – W-type optical fibers with two and three claddings and a step-index profile. The cross-section of the refractive index profile of a W-type optical fiber is shown in Figure 25. W-type optical fiber consists of four glass regions: a large central core (35 μm) with highest refractive index n_1 surrounded by an extremely thin cladding having a least refractive index n_2, the role of which is to preserve only the fundamental mode in the core; two claddings with refractive indices

$n_3 < n_4$, respectively, for maintaining the fiber resistance for propagation of a high-intensity beam. The profile of the refractive index n of such optical fibers makes it possible to vary a large number of fiber parameters and efficiently filter higher modes by changing the refractive index n_3 and n_4.

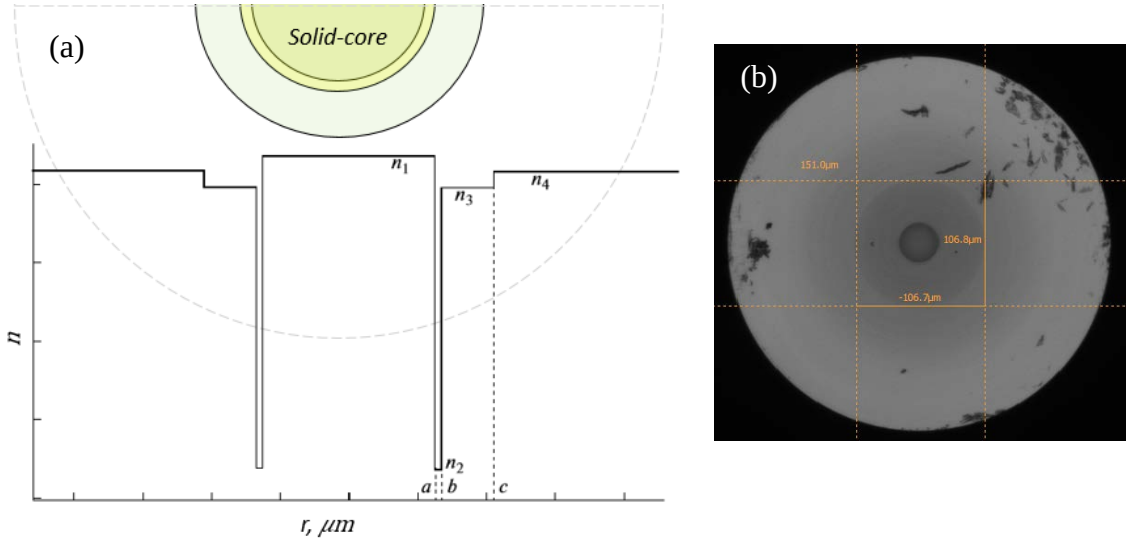

Fig. 25. Representation of (a) the refractive index profile and (b) the cross-section for the fabricated sample of a W-type delivery optical fiber.

The experimental study includes the investigation of six delivery fiber samples. Their geometrical parameters are presented in Table 1. All samples were manufacturing by the same method described in the next section.

Table 1. Summary of the fiber samples geometric parameters: the diameters of the cores, claddings and lengths for delivery optical W-type fibers

W-type optical fiber sample	Core diameter (n_1 area), μm	The diameters of the claddings with refractive indices n_2, n_3 and n_4, respectively, μm	Length, m
Sample 1	35	39/323/450	5
Sample 2	35	39/110/315	4.2
Sample 3	35	39/323/450	2.8
Sample 4	45	51/142/405	2.7
Sample 5	32	40/100/288	4
Sample 6	30	38/94/270	4.8

6.2 Manufacturing process of the all-glass W-type delivery fiber for ultra-high power laser system

All-glass W-type delivery fiber with a large mode area (LMA) maintain their waveguide properties according to the law of the total internal reflection (TIR) [33]. The confinement of the fundamental mode only is enabled by establishment of leaking channels for higher-order modes along the light propagation. Such fibers are much easier to manufacture in comparison, for example, with photonic crystal fibers [47] or photonic band gap fibers (the current state-of-the art for the delivery fibers) [10] due to all-glass structure.

The manufacture process consisted of two principle steps: a preform fabrication and a fiber drawing. The preform was a glass rod, the diameter of which can be from 1 to 10 cm and a length from 1 to 2 m. It included a core rod and several tubes with different refractive indices according to the specified design, which are stacking together. A core was fabricated by modified chemical vapor deposition process. The essence of the method was that a mixture of oxygen, silicon tetrachloride ($SiCl_4$) etc. was passed through a rotating quartz glass tube, heated externally by a flame to a temperature of approximately 1600 °C.

Chemical reactions that occur in the gas inside the tube produced a precipitate of silica, which covered the interior surface of the glass tube near the burner and was sintered into a transparent layer of glass. The burner was in constant forward and backward motion along the tube. As a result, a layer with a higher refractive index was formed. The outer glass tube broke when heated to a temperature of approximately 2000 °C [10]. The preform fabrication process was accomplished by sintering the tubes' assembly under high temperature. Then, the preform was established in the special holder of fiber drawing tower, where it was heated up and a fiber was pulled out under gravity effect. The photo of the preform and schematic presentation of the fiber-drawer tower is shown in Figure 26.

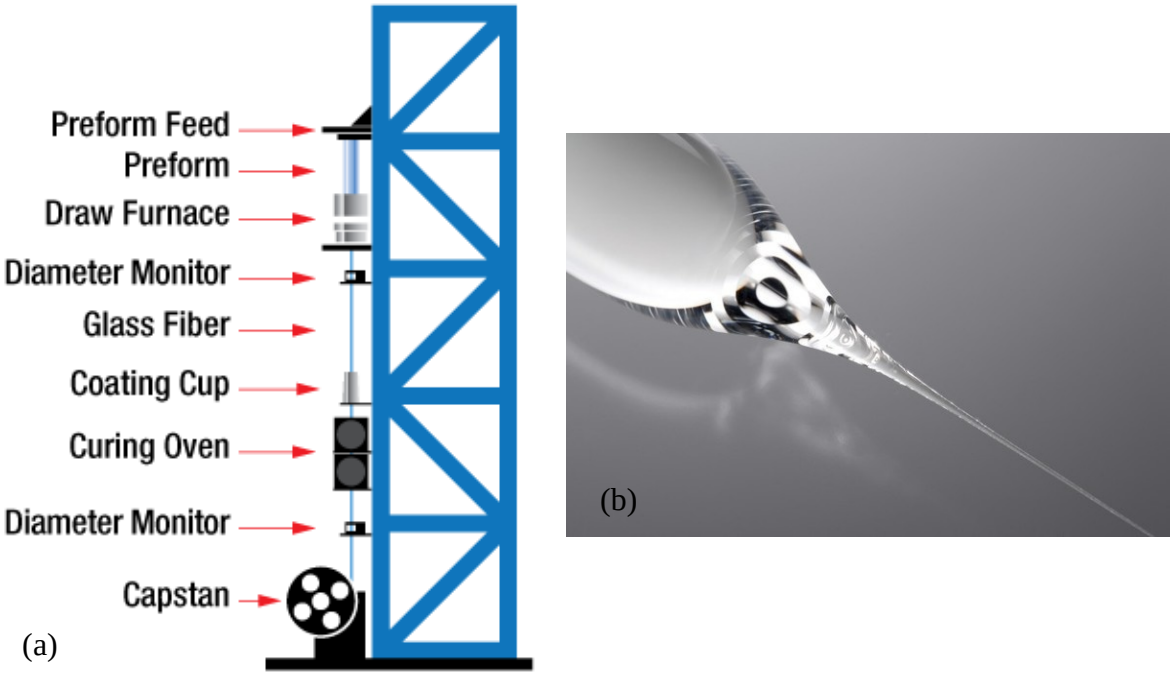

Fig. 26. (a) The **s**implified sketch of fiber drawing tower [25] and (b) the sample preform [54].

Before winding, the fibers were covered by a polymer coating for mechanical and chemical protection. These coatings consisted of several layers for optimal suppression of fiber microbends [10].

6.3 Characterization of a W-type delivery optical fiber

The most important parameters of a fiber are optical losses and attenuation of the transmitted energy, showing how much the signal level at the output of the optical fiber has decreased in comparison to the input level. These parameters determine the transmission range of a high-power signal through an optical fiber and its effectiveness. An understanding of the main causes of losses in the optical fiber is necessary in order to ensure their elimination and high-quality control of the materials used for the manufacture of optical fibers.

6.3.1 Bending losses

Definition

The losses of an optical power as light propagates through the core of the W-type optical fiber is called the attenuation, which is determined by the ratio of the optical powers at the output P_{out} and the input P_{in} of the optical fiber. Attenuation is influenced by factors such as intrinsic losses (losses on absorption in the fiber material, scattering losses) and additional losses (waveguide losses). Losses due to absorption are directly related to the presence in the fiber material (silica glass) of various impurities of metals and hydroxyl ions [55].

Losses due to Rayleigh scattering in a fiber are caused by light scattering on microinhomogeneities with sizes smaller than the wavelength of light in a fiber, which occur during fiber manufacturing due to fluctuations in the density and composition of silica glass (Fig. 27) [56].

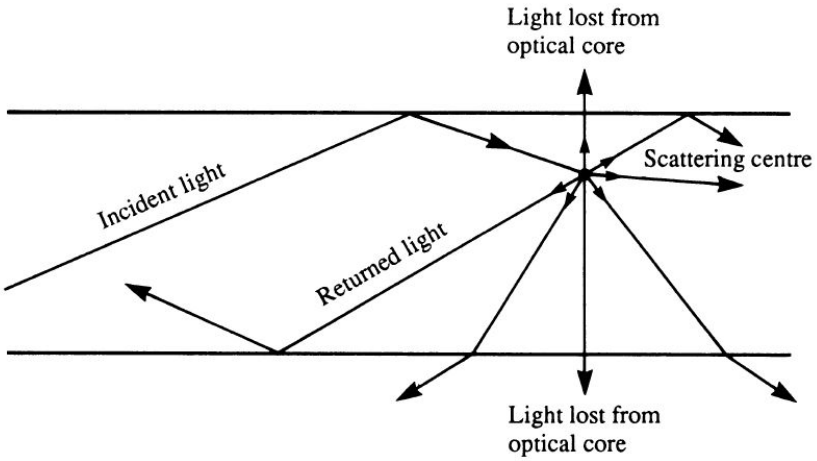

Fig. 27. Rayleigh scattering in optical fiber, occurring in all directions [57].

In reality, the density of the glass is not uniform. As a consequence, scattering occurs in all directions. These losses are of fundamental character; they present in all types of fibers and limit the minimum achievable attenuation in the fiber. Rayleigh losses are highly dependent on the radiation wavelength; the attenuation coefficient due to Rayleigh losses is inversely proportional to the fourth power of the wavelength λ [56].

During the fabrication and exploitation of an optical fiber, operational losses may occur. They are caused by twisting, deformation and bending the fibers during protective polymer coating [56].

Due to different propagation conditions of the light wave in the conventional and bended conditions in the fiber, additional losses of radiation power can occur, leading to a corresponding attenuation of the light. Figure 28 shows the pathway of the rays during the propagation of light in a fiber with microbends and in a bended fiber. Microbends can occur due to the presence of roughness at the boundary of the protective-hardening coating of the fiber and the outer cladding during fiber compression. From the Figure 28 it is seen that the presence of those and other bends leads to the emission of light into the cladding and additional attenuation. In addition to microbends, the insertion loss also includes losses associated with defects in optical fibers (cracks, bubbles, microinhomogeneities) [58]. Macrobends losses are associated with the fiber spooling. They determine the minimum spool diameter of the fiber.

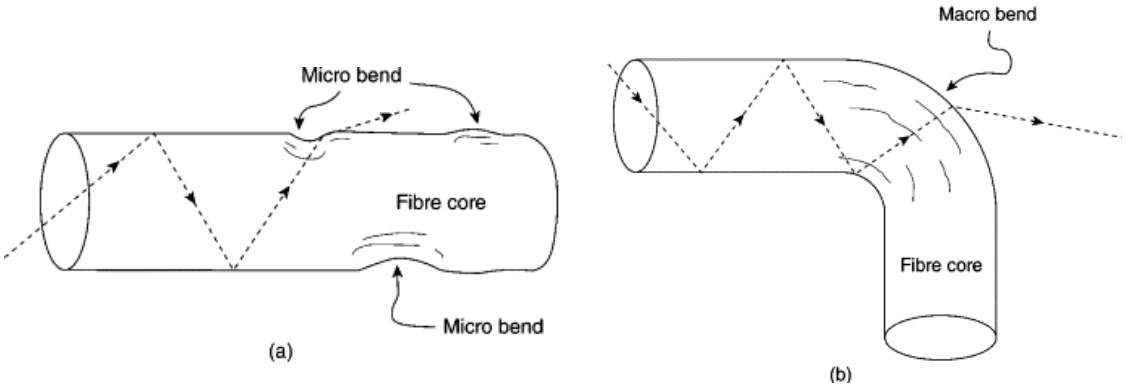

Fig. 28. Presence of losses in the optical fiber due to (a) micro bends, (b) macro bends [58].

The loss of an optical power as light propagates through the fiber is characterized by the attenuation coefficient α, which is determined by the ratio of the optical radiation powers at the input P_{in} and the output P_{out}. The attenuation coefficient α is measured in decibels per millimeter (dB/mm) and it can be found from the equation:

$$\alpha\left(\frac{dB}{mm}\right) = \frac{10ln\left[\frac{P_{in}}{P_{out}}\right]}{l}, \tag{13}$$

where α is attenuation coefficient, which characterizes the loss of radiation power in optical fibers, P_{in} and P_{out} are the optical radiation powers at the input and output of the fiber, respectively and l is fiber length [56].

The attenuation coefficient α is determined by the intrinsic absorption losses, Rayleigh scattering of light in the fiber, and the introduced losses caused by micro- and macrobending, as well as artificial fiber defects [56].

To evaluate input P_{in} and output P_{out} powers, it is convenient to use the most common, simple and widely used loss-measuring instrument, called optical power meter. Usually it is made with the ability to indicate power both in absolute (W, mW, μW, nW) and in relative (dB, dBm) units. An optical power meter is the primary instrument for conducting fiber optic measurements. Thanks to different types of photosensitive sensors (usually a photodiode), optical power meters can operate in various spectral ranges required for various applications.

So, power meters designed for testing optical fibers use silicon (well operating at a wavelength of 850 nm), germanium (spectral range of operation – 1300-1500 nm) or gallium-indium-arsenide (850-1550 nm) photodiodes. Therefore, when choosing a power meter, it is necessary to pay attention to the dynamic measurement range of the device.

Experimental setup

In this work, the measurements were focusing on evaluation of the bending loss occurred in a single-mode W-type delivery optical fiber with a large mode area. Since the intrinsic losses are similar for all samples, the bending losses in their turn determine the minimum acceptable bend diameter for the fiber which is important characteristic for a delivery fiber. In order to measure the bending losses in a W-type optical fiber, we used a setup whose simplified diagram is shown in the Figure 29.

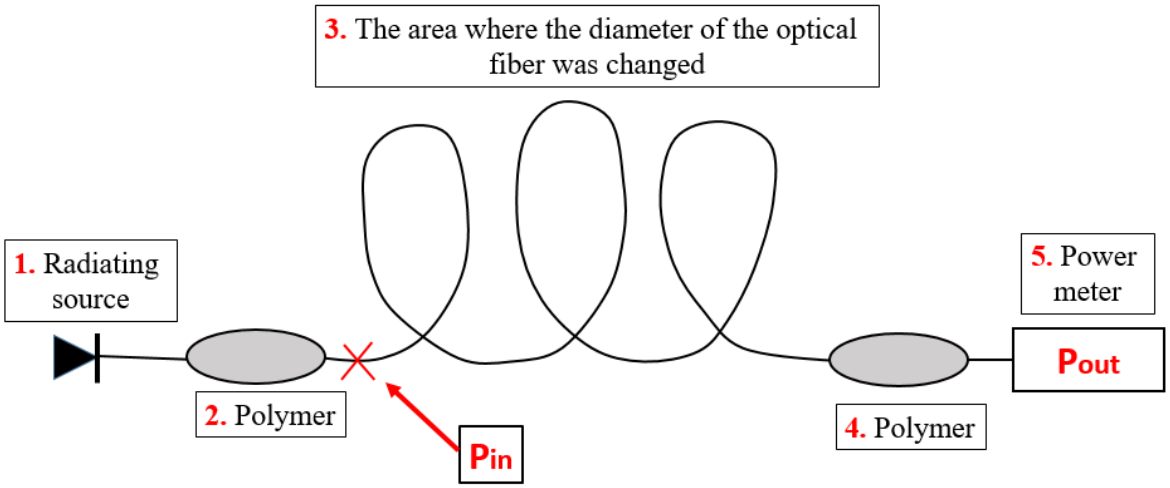

Fig. 29. A simplified scheme for measuring bending loss in an optical fiber.

The setup includes two basic elements for the experiment, the first of which is a radiating source (1) represented by a "Butterfly" diode (Fig. 30) with a fiber pigtail output [59]. A “Butterfly” diode consists of a laser diode, an integrated Peltier thermoelectric cooler, a thermistor and a photoelectric tracking device. The Peltier element is a thermoelectric converter, the principle of which is based on the Peltier effect: the occurrence of a temperature difference during the flow of electric current [1]. The main difference between “Butterfly” diode from others is that it provides a more efficient heat sink of the laser diode

due to the increased contact area of the Peltier element with the laser module housing (the main heat sink surface is at the bottom). For effective heat removal, the electrical leads are moved to the side faces. These “Butterfly” diodes are widely used in fiber optics. In our case, the butterfly diode was designed for a wavelength of 976 nm.

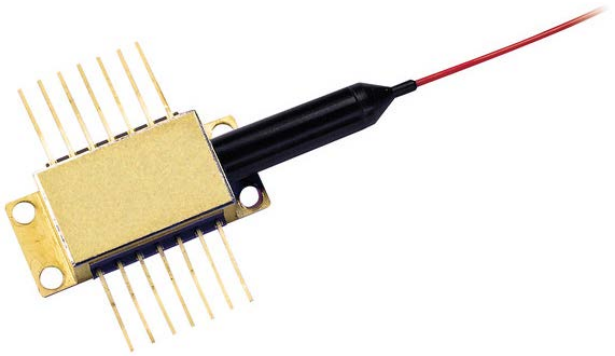

Fig. 30. “Butterfly” diode, used as a radiating source in an experimental setup for measuring bending loss in an optical fiber [59].

Second important element used in the setup for the measurement of bending loss in a W-type optical fiber is a power meter recording the changes in output power (5).

The working principle of the setup is that the “Butterfly” laser diode emits a light beam at a wavelength of 976 nm that passes through a W-type delivery optical fiber, and then the magnitude of the transmitted radiation is recorded by a power meter.

An important role belongs to the so-called cladding mode stripper (or polymer 2, 4), shown in the Figure 29. The cladding mode stripper is a filter for higher-order modes propagating in the optical fiber. The higher-order modes excited at the fiber input eventually “flow out” from the fiber core to the cladding area during propagation. Due to the presence of the polymer as an outer layer of the optical fiber, these modes exit fiber through the polymer into the air as TIR condition is not functional at the border, where light penetrate to the layer with higher refractive index. If there is no polymer, the modes would propagate into the fiber cladding and their power would be counted at the power meter. Thus, using the polymer, we ensured the propagation of the fundamental mode only along the core of the optical fiber.

Bending loss for a W-type delivery optical fiber was investigated as follows. First, it is necessary to measure the input power P_{in} using a power meter specifically at the point indicated in the Figure 29. As mentioned earlier, the polymer provides filtering higher-order modes, ensuring the propagation of the fundamental mode along the fiber core. Exactly this power of the fundamental mode should be registered by the power meter as the input power P_{in}. As shown in the Figure 29, the W-type optical fiber was bent into rings with different diameters, and then the output power P_{out} was recorded by a power meter. In case of high fiber sensitivity to the bending the fundamental mode should leak to the cladding and through high index polymer to the air resulted in high variation of the output power. In case of strong field confinement in the fiber core the output power will demonstrate a week dependence on the bending.

Measurement results

Bending loss were measured in six W-type delivery optical fiber samples presented in the Table 1. All samples fibers were bent into rings of different curvatures *d*: 500, 400, 300, 200 and 100 mm; for each sample the resulting output powers were recorded. Figure 31 (a) – (f) show the dependences of the change in output power with decreasing fiber curvature. The experimental results were carried out at different powers of the emitting source P_{source}; for the convenience of representation, the results for each sample are placed on the separate graphs.

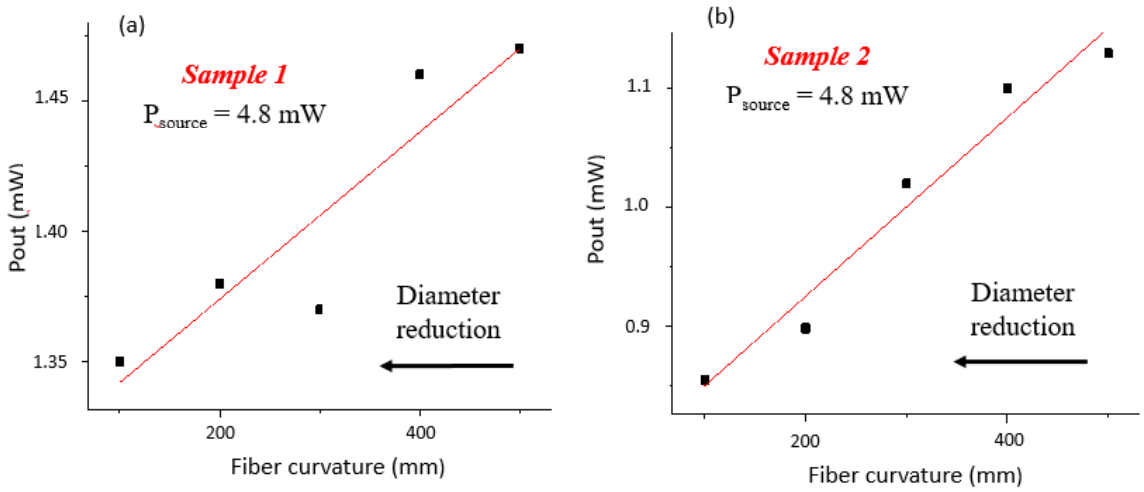

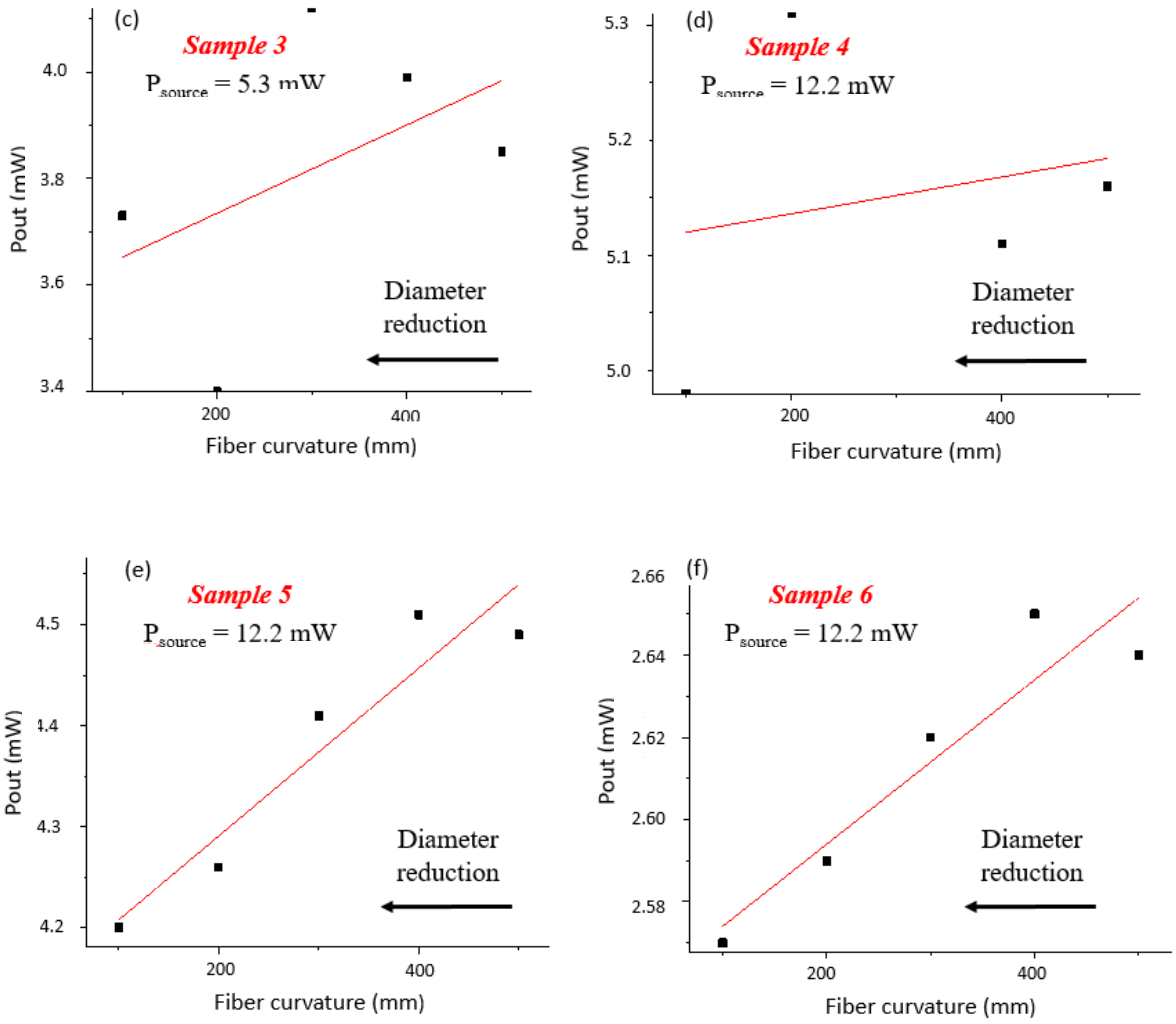

Fig. 31. Dependence of the bend-associated losses on the bending diameter for six W-type delivery optical fiber samples.

The input power P_{in} was measured at the most direct fiber arrangement for each sample separately. This approach allows including the intrinsic losses of the fiber's sample. The measurement results are summarized in Table 2.

Table 2. Measurements of input power with the most direct fiber arrangement for all six samples

	Sample 1	Sample 2	Sample 3	Sample 4	Sample 5	Sample 6
P_{in}, mW	1.5	1.3	4.2	5.32	4.52	2.7

Using the formula (13), it is possible to calculate the bending loss for each sample. The calculated values of the attenuation coefficients, α, are presented in the Table 3.

Table 3. The calculated values of attenuation coefficients, α, for various delivery optical W-type fiber diameters

	d, mm	500	400	300	200	100
Sample 1	***α, dB/mm***	0.000040	0.000054	0.000181	0.000167	0.000211
Sample 2	***α, dB/mm***	0.000334	0.000398	0.000578	0.000881	0.001001
Sample 3	***α, dB/mm***	0.000311	0.000183	0.000069	0.000755	0.000424
Sample 4	***α, dB/mm***	0.000113	0.000149	0.000085	0.000007	0.000245
Sample 5	***α, dB/mm***	0.000017	0.000006	0.000062	0.000148	0.000184
Sample 6	***α, dB/mm***	0.000047	0.000039	0.000063	0.000087	0.000103

The measurements showed that a decrease in the ring diameter of the fiber d leaded to only slight attenuation of the output power P_{out}, as a consequence, the attenuation coefficient α varied negligibly. Thus, all samples demonstrated weak sensitivity to the bending, which is an indicator of the strong localization of the field in the fiber core.

6.3.2 Beam divergence and mode field diameter

Measurement techniques

The propagation of optical radiation along an optical fiber is based on the phenomenon of total internal reflection (TIR) at the interface of media with different refractive indices [33]. The process of propagation of light rays in an optically denser medium, a core with highest refractive index n_1, surrounded by a less dense one, a cladding with lower refractive index n_2, is shown in Figure 32.

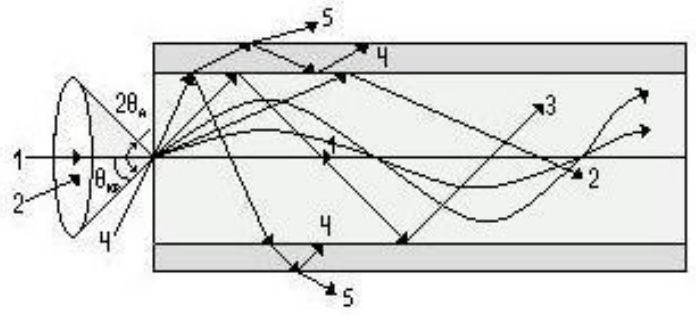

Fig. 32. Demonstration of the propagation of guided (rays 1 - 3), leaking (4) and emitted (5) light rays through an optical fiber [60]

The angle of total internal reflection (TIR), at which the radiation incident on the boundary of an optically denser and optically less dense medium, is completely reflected, is determined using the ratio (4) from the section 4.1 [32].

When light enters the fiber end, three types of light rays can propagate in it: guided, leaking and emitted rays. The presence and predominance of any type of rays is determined by the angle of their incidence at the core – cladding interface. Those rays that fall at the interface at an angle $\Theta \leq \Theta_{critical}$ (rays 1, 2 and 3 in the Figure 32) are reflected from it and return to the fiber core, propagating in the core and not undergoing refraction. Since the trajectories of such rays are completely located inside the propagation medium, the core of the fiber, they propagate over long distances and are called guided [60].

Rays falling on the interface at angles $\Theta > \Theta_{critical}$ (rays 4) are called leaking rays (cladding rays). Reaching the core – cladding boundary, these rays are reflected and refracted, each time losing part of the energy to the fiber cladding, and therefore disappear altogether at some distance from the fiber end [60].

Rays that are emitted from the cladding into the surrounding space (rays 5) are called emitted rays and arise in places of irregularities or due to twisting of a fiber. Emitted and leaking rays are spurious and lead to energy dissipation and distortion of the output signal.

The radiation is coupled at a slight angle into the end of the optical fiber. The maximum angle of input of the light pulse are able to enter into the fiber core is called the numerical aperture (NA) of the optical fiber, which is calculated by the formula (5) from the section 4.3. From this formula follows that the numerical aperture (NA) of the fiber depends only on the refractive indices of the core n_1 and cladding n_2. In this case, the condition $n_1 > n_2$ is always satisfied.

The radiation propagating through an optical fiber can have different spatial and angular distributions depending on the excitation of the fiber modes. To get useful information about the fiber is possible by analyzing the radiation that comes out from the fiber end. Such analysis can be carried out both in the far- and near-fields of the fiber end. Using the measurement of the far-field, it is possible to determine the angular dependence of the intensity at a far distance from the fiber end (Figure 33 (a)), i.e. the divergence of the light beam Θ, and then knowing the divergence Θ, the mode field diameter (MFD) of the light beam can be calculated. Using the near-field measurement it is also possible to determine the spatial intensity distribution in the plane of the fiber end, i.e. the mode field diameter (MFD) [61].

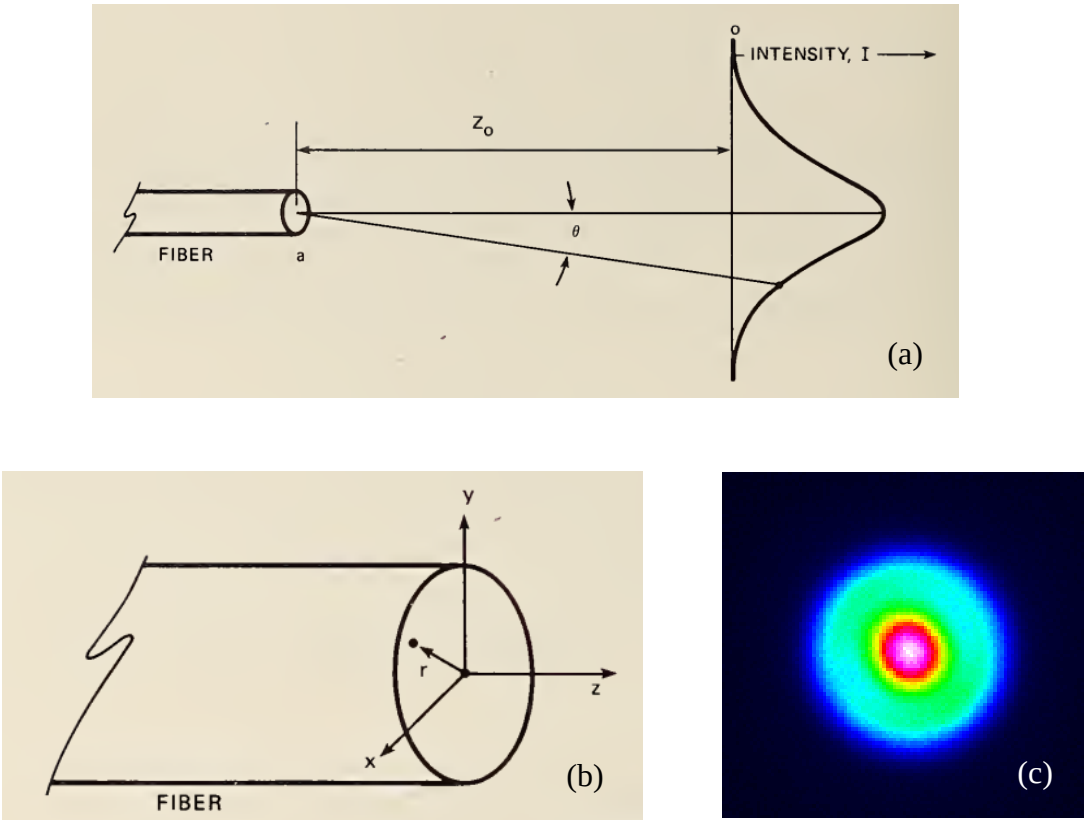

Fig. 33. Schematic representation of (a) a far- and (b) a near-field measurements [61]; (c) an intensity distribution for a near-field measurement technique.

The method for measuring the mode field diameter (MFD) directly at the end of the optical fiber is called the near-field technique (Fig. 33 (b) – (c)). This method uses an objective lens which focal plane is located at the end of the fiber. The profiling device analyzes the resulting image of the beam; the camera gives the image containing information about the mode field diameter (MFD) (Fig. 34 (a)). The camera can perform near-field measurements by registering the size of the mode field with the cursor, as shown in Figure 34 (b). The numerical value for the field diameter of the mode d_{core} at the end of the optical fiber that is obtained using special software is a computer approximation, and not the true size of the mode field. The real size of the mode field (MFD) is necessary to calculate.

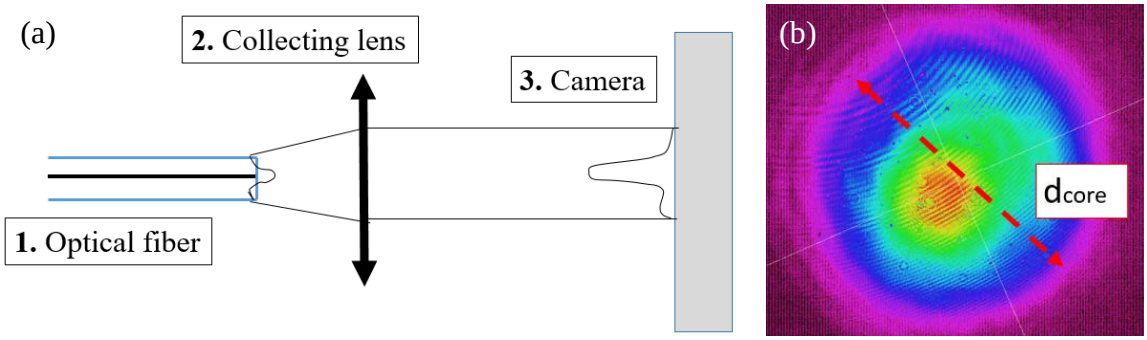

Fig. 34. Representation of (a) the characterization of the MFD by near-field measurements for W-type delivery optical fiber and (b) the picture of the MFD, the size of which is determined using the camera.

However, near-field technique is not accurate. This is because such method requires a high level of positioning accuracy, which is a technical challenge.

A more precise and reliable method to determine the mode field diameter (MFD) is the far-field technique, which allows calculation of the MFD through the divergence Θ of the light beam [62].

The near- and far-field measurements can be performed using an optical camera and special software, where the calculation of the mode field diameter (MFD) is based on two methods: “The $1/e^2$ width” and “The 4 Sigma”. The description of these methods is given below.

“The $1/e^2$ width” method measures the beam width between two points, where the intensity is $1/e^2$ of the peak value. This is a relatively clear definition of the mode size, since only about 86 % of the laser power is contained within a width of $1/e^2$. “The $1/e^2$ width” method is used to calculate the diameter of a Gaussian beam in single-mode optical fibers. A Gaussian beam is a coherent light beam with a Gaussian field distribution, which is fundamental in the theory of wave beams. This beam is called the fundamental (main) mode, unlike other modes of a higher order [53]. The schematic of “The $1/e^2$ width” method determining the magnitude of the electromagnetic field for a Gaussian beam is shown in Figure 35.

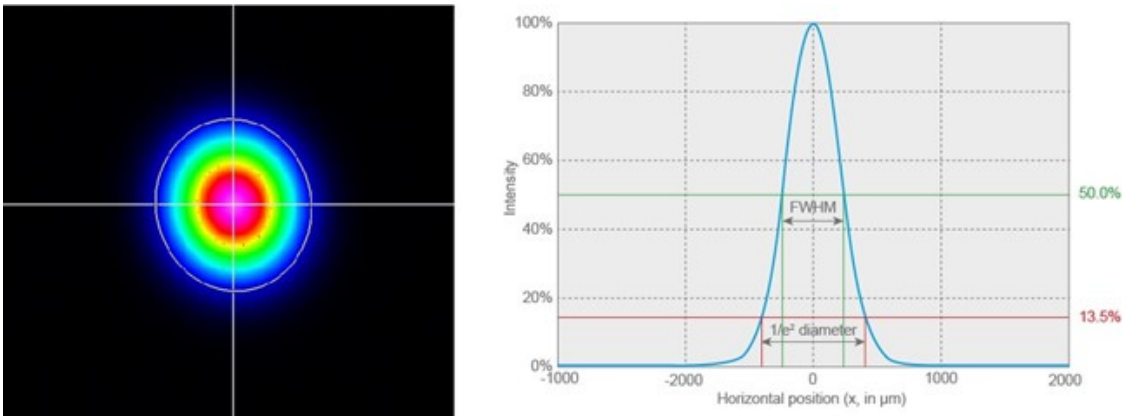

Fig. 35. "The $1/e^2$ width" method presentation to determine the magnitude of the electromagnetic field for a Gaussian beam [53].

For an arbitrary (possibly non-Gaussian) beam shape, it is recommended to use a method called "The 4 Sigma" method. Here, the beam width in the horizontal or vertical direction is 4 times greater than σ, where σ is the standard deviation of the horizontal or vertical intensity distribution, respectively. The radius of the beam is described by the equation:

$$w = 2 \times \sqrt{\frac{\int x^2 I(x,y)\, dx\, dy}{\int I(x,y)\, dx\, dy}}, \tag{14}$$

where the x and y coordinates should be taken relative to the center of the beam [26]. The x and y coordinates are used to describe the distribution of the mode field in two-dimensional space. For Gaussian beams, "The 4 Sigma" method gives the same result as the $1/e^2$ method, while for other beam shapes there can be significant deviations.

Also it should be noted the meaning of the term divergence θ of the light beam. Beam divergence θ is an angular measure of the increase in the diameter or radius of a beam with the distance when the beam exits the fiber. The term is relevant only to the far field, outside of any beam focusing [61].

Experimental setup and measurement results

Using far-field measurements, we calculate the divergence θ of the light beam emitted from the optical fiber as follows. The end of the fiber is placed on a special optical table. On the same table we attach an optical lens to obtain a collimated beam of light. A beam of light is emitted from the fiber, passes through an optical lens and hits a camera that measures the size of the electromagnetic field of radiation. By moving the camera at equal distances from the optical stage with the fixed fiber, the size of the electromagnetic field was recorded by two methods, "The 4 Sigma" method and "The $1/e^2$ width" method. An optical fiber laser with a wavelength of 1047 nm was used as a radiation source. The divergence of the light beam was calculated both for a conventional single-mode optical fiber coming from a fiber-optic laser and for the delivery W-type fiber. A schematic diagram for measurement of the divergence θ of a light beam is shown in Figure 36 (a).

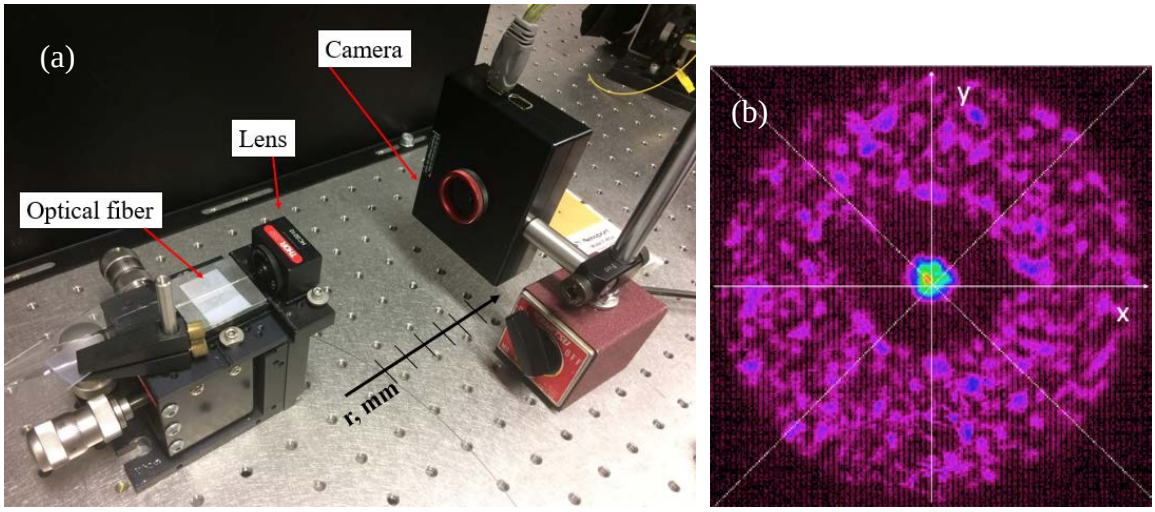

Fig. 36. (a) The experimental setup to measure the divergence of a light beam by using the far-field measurement technique and (b) a far-field image for a single-mode fiber of a radiation source.

Firstly, the calculation of the divergence θ of a light beam for a single-mode fiber coming from a radiation source was performed. During the experiment, the camera was moved several times from the optical stage with the fiber to a distance r equal to 2.5 mm; the electromagnetic field was measured in two ways, "The 4 Sigma" method and "The $1/e^2$

width" method. The image of the far-field measurement after the propagation of a light beam through a single-mode optical fiber of a laser source is shown in the Figure 36 (b).

The results of the experiment are presented in Figure 37. The field diameter was measured as a function of the distance *r* between the camera and the optical stage with the single-mode optical fiber in two coordinates: *x* and *y*. To compare the results of "The 4 Sigma" and "The $1/e^2$ width" methods, we construct the values for the *x* values on one graph, and the *y* values on the other graph for the two methods, respectively. The measurements obtained using "The 4 Sigma" method are shown with black dots, and "The $1/e^2$ width" method with green dots. The values in Figures 37 (a) – (b) are presented in millimeters.

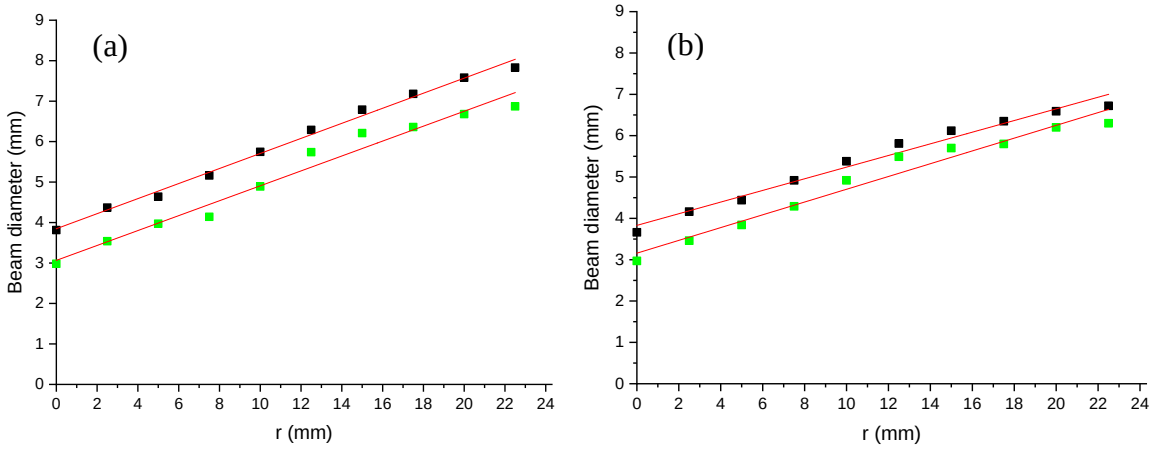

Fig. 37. Dependences of the beam diameter (black dots show "The 4 Sigma" method and green dots show "The $1/e^2$ width" method) on the position of the fiber-camera (*r*). Results presented in (a) x-direction (b) y-direction.

The camera was moved with same step for all measurements to ensure the procedure similarity. Having the beam size variation with the distance and using basic geometric approach, we can calculate the divergence of the field θ as follows. Figure 38 (a) shows the divergence of a light beam θ emitted from an optical fiber. d_1, d_2, d_3, etc. are the measured quantities, which are the diameters of the mode field recorded by the camera at the same intervals (distances) r_1, r_2, r_3, etc. Figure 38 (b) shows a linear dependence of the obtained values for the mode field diameter depending on the distance between the camera and the optical stage with the optical fiber. On the horizontal axis there are equal intervals of

distances r_1, r_2, r_3, … in millimeters, on the vertical axis are the corresponding dimensions of the field diameter in millimeters, respectively.

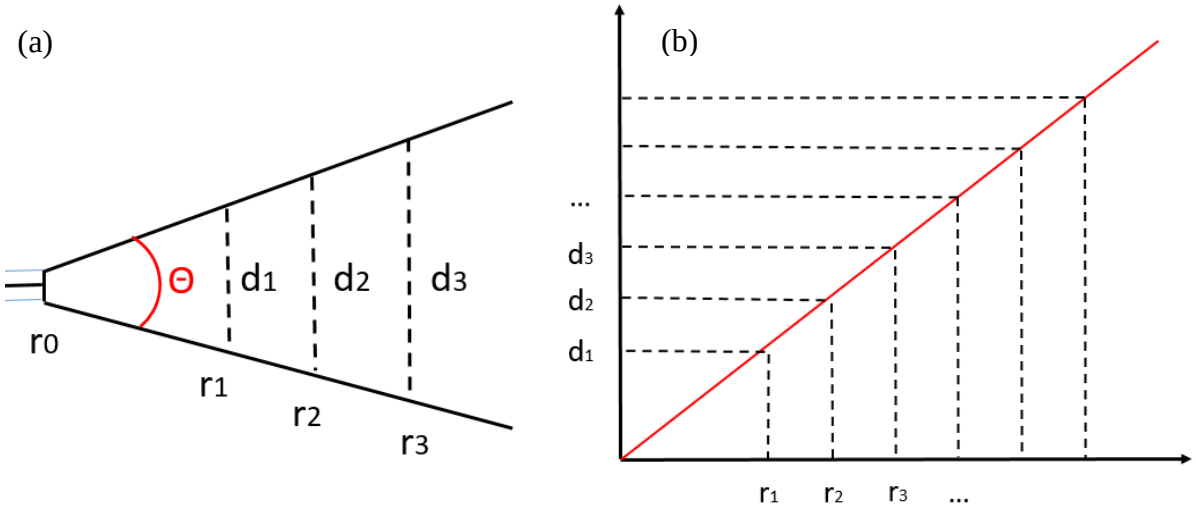

Fig. 38. (a) Representation of variation of the beam divergence versus camera-optical fiber distance, (b) Linear approximation of the dependence of the beam divergence on the distance of the camera-optical fiber.

According to the linear dependence of the mode diameter on the distance between the camera and the fiber end, the slope angle can be determined geometrically. The slope angle is the beam divergence θ. Using the geometric method, we can write an equation that describes the linear approximation

$$d = k \times r + b \,, \tag{15}$$

where the coefficient k is the angular coefficient of the line, calculated by the following formula:

$$k = tg\,\theta \,. \tag{16}$$

Therefore, from the linear approximation of the measurement results shown in Figure 37 (a) – (b) it is possible to calculate the divergence of the light beam using the geometric ratio. The corresponding results are presented in Table 4.

Table 4. Estimation of the divergence by two methods: "The 4 Sigma" and "The $1/e^2$ width" (for single mode fiber)

	"The 4 Sigma" method		**"The $1/e^2$ width"** method	
	X-value	Y-value	X-value	Y-value
Θ, mrad	186.1	141.7	184.5	184.1

Knowing the values of the light beam divergence θ and the wavelength, we can determine the mode field diameter (MFD). As a rule, MFD is larger than the physical diameter of the fiber core, which means that some optical power is always propagated in the fiber cladding. The mode field diameter for a single-mode optical fiber can be determined using the expression for a Gaussian beam [58]:

$$MFD = \frac{4\times\lambda}{\pi\times\theta}. \quad (17)$$

The MFD values calculated for the two methods, "The 4 Sigma" and "The $1/e^2$ width", are presented in the Table 5.

Table 5. Estimation of the mode field diameter by two methods: "The 4 Sigma" method and "The $1/e^2$ width" method (for single mode fiber)

	"The 4 Sigma" method		**"The $1/e^2$ width"** method	
	X-value	Y-value	X-value	Y-value
MFD, μm	7.1669	9.4125	7.2290	7.2447

The MFD is important because it is a "measure of conformity" for two optical fibers: source fiber and W-type delivery fiber. The knowledge of the beam divergence θ and the mode field diameter allows selecting of an optical lens system for efficiently launching light from a radiating source to a W-type delivery fiber (this will be discussed in the section 6.4).

Now similar approach will be applied to estimate the MFD for the Sample 1 of W-type delivery optical fiber.

During the experiment, the same distance intervals were settled as for the previous fiber. The camera was moved with the step *r* equal to 2.5 mm and the mode field diameter was measured using "The 4 Sigma" and "The $1/e^2$ width" methods. In the similar way, we express the results of these two methods on two graphs: for x-values, on the other for y-values. Linear approximations are shown in Figures 39 (a) – (b). The measurements obtained using "The 4 Sigma" method are shown with black dots, and "The $1/e^2$ width" width method with green dots. The results are indicated in millimeters.

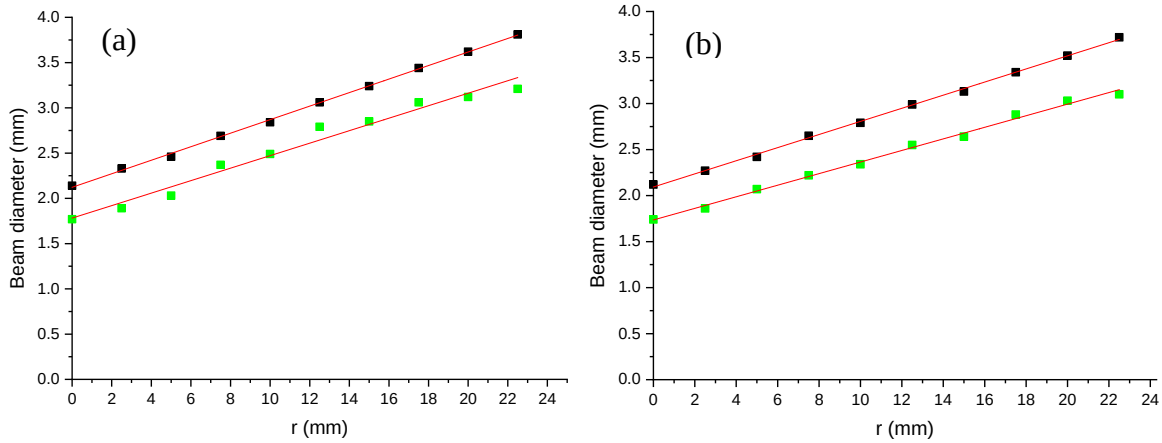

Fig. 39. Dependences of the beam diameter (black dots show "The 4 Sigma" method and green dots show "The $1/e^2$ width" method) on the position of the fiber-camera (*r*). Results presented in (a) x-direction (b) y-direction.

From the data shown in Figure 39 (a) – (b), we calculated the divergence θ of the light beam using the geometric relation (16). The corresponding results are presented in the Table 6.

Table 6. Estimation of the divergence by two methods: "The 4 Sigma" and "The $1/e^2$ width" (for the Sample 1 W-type fiber)

	"The 4 Sigma" method		**"The $1/e^2$ width"** method	
	X-value	Y-value	X-value	Y-value
Θ, mrad	82.90	86.10	68	73.42

The next step is the calculation of the mode field diameter (MFD) for the two methods: "The 4 Sigma" and "The $1/e^2$ width". The results are presented in the Table 7.

Table 7. Determination of the mode field diameter by two methods: "The 4 Sigma" and "The $1/e^2$ width" (for the Sample 1 W-type fiber)

	"The 4 Sigma" method		**"The $1/e^2$ width"** method	
	X-value	Y-value	X-value	Y-value
MFD, μm	16.4097	15.4468	19.9141	18.1661

Using similar calculations for the far-field measurement technique, we find the divergences of the light beams and the mode field diameter for each of the six samples of the W-type delivery optical fiber. The results for all samples are presented in the Table 8.

Table 8. The calculated results of the divergence of the light beam and the mode field diameter for six samples of the W-type optical fiber

		"The 4 Sigma" method		**"The 1/e^2 width"** method	
		X-value	Y-value	X-value	Y-value
Sample 1	*Θ, mrad*	82.90	86.10	68	73.42
	MFD, μm	16.4097	15.4468	19.9141	18.1661
Sample 2	*Θ, mrad*	113.88	141.74	90.41	97.49
	MFD, μm	11.7120	9.4099	14.7523	13.6810
Sample 3	*Θ, mrad*	132.93	142.87	42.3	43.15
	MFD, μm	10.0335	9.3355	31.5309	30.9098
Sample 4	*Θ, mrad*	135.27	139.31	96.65	123.57
	MFD, μm	9.8599	9.5740	13.7999	10.7935
Sample 5	*Θ, mrad*	90.95	115.77	78.12	88.78
	MFD, μm	14.6647	11.5208	17.0732	15.0232
Sample 6	*Θ, mrad*	88.5	109.86	77.47	90.45
	MFD, μm	15.0707	12.1405	17.2164	14.7458

Due to the fact, that the near-field measurement technique is not as accurate as the far-field because of the difficulty of precise positioning, we present the calculation using the near-field method only for the Sample 1 to compare the results of the two techniques. As mentioned earlier, the camera measures the size of the field using the cursor, as shown in Figure 34 (b). The numerical value for the field diameter of the mode d_{core} at the end of the optical fiber, obtained using special software is approximately 1.762 mm; but this value only is a computer approximation, and not the true size of the mode field. The approach for calculation of the real size of the mode field diameter (MFD) is described below.

First, we recorded the near-field values for the beam diameter $d_{camera\ value}$ using camera by two methods that described above: “The 4 Sigma” and “The $1/e^2$ width”. The obtained numerical values are indicated in the Table 9.

Table 9. The calculated near-field values of the beam diameter by two methods: The 4 Sigma” and “The $1/e^2$ width”

	“The 4 Sigma” method		**“The $1/e^2$ width”** method	
	X-value	Y-value	X-value	Y-value
$d_{camera\ value}$, mm	0.91	0.89	0.87	0.88

We know the real core diameter $d_{actual\ core}$ of the Sample 1 W-type delivery optical fiber, which is 35 μm. The actual size of the MFD can be estimated by the simplest mathematical method, the method of proportions. So, we have three necessary measurements to calculate the MFD: beam diameter, approximately determined by the camera using the cursor; values characterizing the size of the field and determined by the camera using methods “The 4 Sigma” and “The $1/e^2$ width”; and finally, the real core size of the W-fiber. Imagine the mathematical solution as a proportion is shown in the Figure 40.

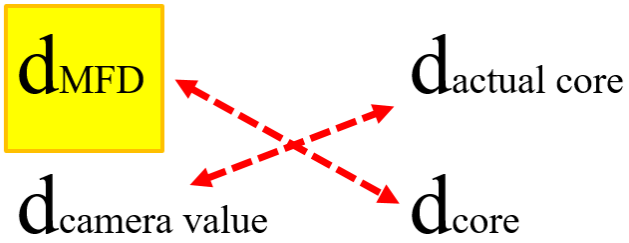

Fig. 40. Calculation of the real size of the mode field diameter using the method of mathematical proportion.

Using the mathematical proportion, we calculated the value for mode field diameter (MFD), which are presented in the Table 10 below.

Table 10. The real size of the mode field diameter calculated by two methods: The 4 Sigma" and "The $1/e^2$ width" (Sample 1).

	"The 4 Sigma" method		**"The $1/e^2$ width"** method	
	X-value	Y-value	X-value	Y-value
d_{MFD} , μm	18.1	17.7	17.3	17.5

Using the far-field measurement technique, the result for MFD (Sample 1) is 16.4 μm. Combining the results obtained by using the far- and near-fields approaches, we can conclude that the real size of the mode field diameter for Sample 1 W-type delivery optical fiber is approximately in the range 16.4 ... 18.1 μm.

The following Figures 41 (a) – (f) shows the images of the mode field distribution at the fiber end for the near-field measurement technique for six samples of the W-type delivery optical fiber. Images of the MFD were obtained using an optical camera. It can be seen from Fig. 41 (a) – (f) that all samples supports single-mode propagation of a fundamental mode through the fiber core.

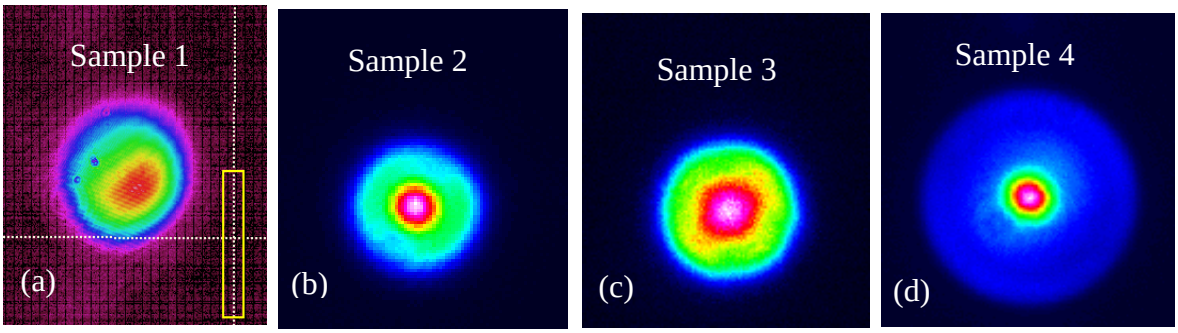

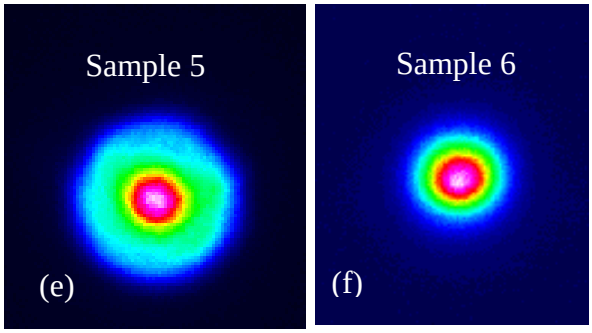

Fig. 41. Images of the mode field distribution at the fiber end by using near-field measurements for six samples of the W-type delivery optical fiber (a) – (f).

6.3.3 Beam quality factor

The laser beam parameter M^2 is a measure of how well the laser beam can be focused with a given angular divergence. This is limited by the numerical aperture of the focusing lens. Together with optical power, the beam quality parameter determines the brightness (more precisely, luminosity) of the laser beam. It is often said about a laser beam that it is M^2 times diffraction limited. The diffraction-limited beam has an M^2 unit, and this is a Gaussian beam. A lower M^2 value is physically impossible [63].

The most common methods to quantify the beam quality are:

• The beam parameter product (BPP) is defined as the product of the smallest beam diameter (beam waist diameter, w_0) and the beam divergence angle measured in the far field. The units for BPP are mm × mrad:

$$BPP = \theta w_0 . \quad (18)$$

• Parameter M^2 indicates how closely the actual laser beam can be focused in comparison with a theoretically perfect Gaussian beam:

$$M^2 = \frac{\pi \theta w_0}{\lambda} . \quad (19)$$

Parameter M^2 can be calculated from measuring the change in the radius of the beam along the propagation axis (i.e., the so-called caustic) [63]. As can be seen from Figure 42,

the caustic is an “envelope” of light rays, bounded by two lines above and below. These two lines do not converge; they have a certain spot of convergence, the diameter of which is called the waist of the light beam. For accurately determination M^2, the beam radius must be measured at several places along the propagation axis.

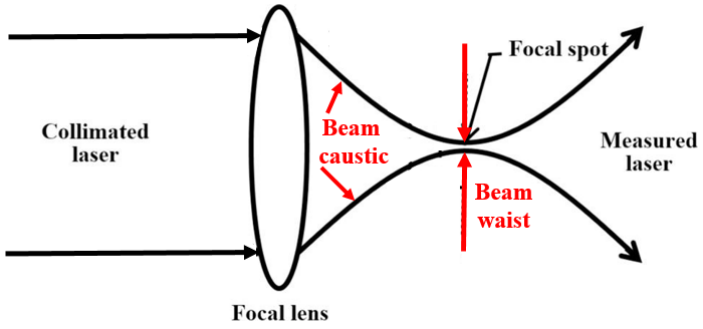

Fig. 42. A schematic of M^2 measurement of the fiber optic laser.

The experimental setup includes an optical fiber laser with a wavelength of 1047 nm, connected to a single-mode fiber, through which radiation passes and enters a W-type fiber. The ends of the fibers are placed in the splicer, as shown in the Figure 43.

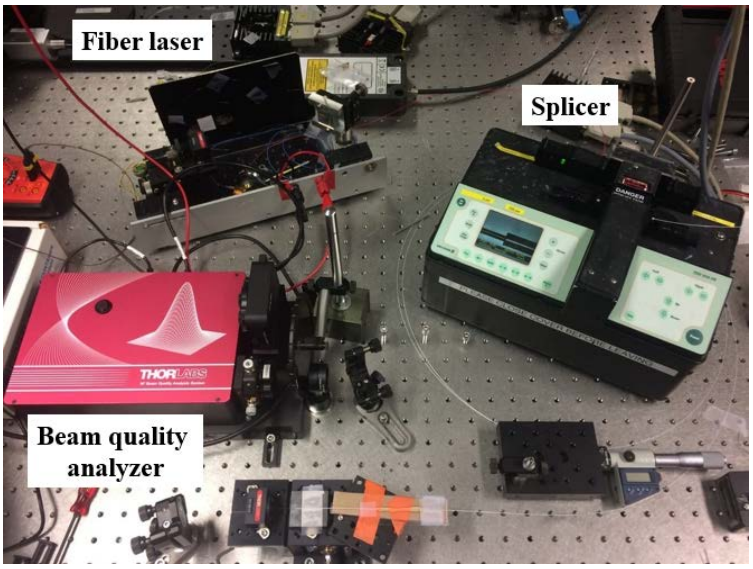

Fig. 43. An experimental setup to determine beam quality parameter M^2.

First of all, it is necessary to collimate the light beam coupling out from the fiber sample. For this, two mirrors are used to align the laser beam with a beam quality analyzer. Then, after passing through the lens, the light beam should be captured by a moving CCD camera (Charge-Coupled Device) in positions that are within two or more Rayleigh lengths on both sides of the beam waist (focal spot). With captured laser intensities, the laser width at the measured positions can be calculated based on the determination of a second-order moment. A change in the beam width depending on the propagation position can be established using a hyperbolic curve, the parameters of which are then used to calculate M^2. During the measurement of the laser beam parameter M^2, the result can be distorted by background light, CCD camera noise, optical element aberrations etc. The scheme for measuring the beam parameter M^2 is shown in the Figure 43. A more detailed diagram of the experimental setup is shown in the Figure 44.

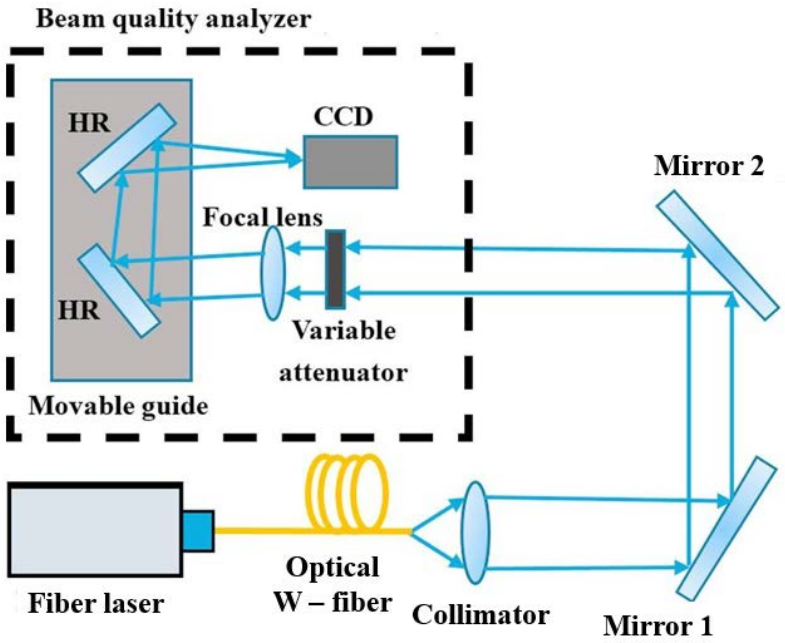

Fig. 44. Schematic of the detailed experimental setup for determining the beam quality parameter M^2 [63].

In the experiment, three segments of the Sample 1 of the W-type optical fiber were considered: 5 m, 10 m, and 15 m. Measurements of the beam quality parameter were first carried out for a fiber length of 15 m; then the fiber was shortened by cutting pieces of 5 m

long fiber to qualify how the light beam quality will evaluate with decreasing fiber length. The measurements of the beam quality parameter M^2 are summarized in the Figure 44. Beam quality parameters M^2min, M^2max and M^2mean were obtained using special software. Values M^2min and M^2max belong to the lower and upper envelopes, respectively (Fig. 42); values M^2mean are the arithmetic average between the maximum and minimum values of the quality parameter of the light beam. This is the value used as a measure of beam quality.

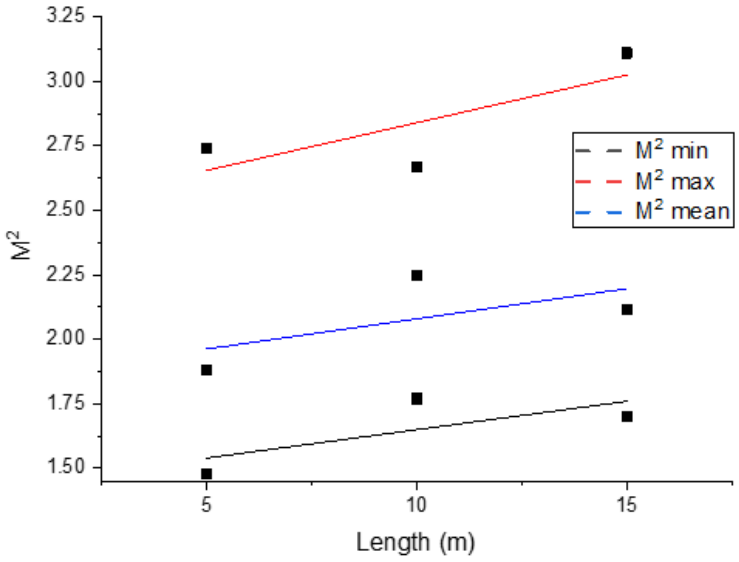

Fig. 45. Linear approximation of the experimental results of the beam quality parameter M^2 for different lengths of the Sample 1.

As can be seen from the Figure 45, the beam quality parameter does not change very much with variation of the fiber length. Consider, for example, the lower envelope having M^2min. The value of the beam quality parameter for a fiber length of 15 m is approximately 1.7; while for the lengths of 10 m and 5 m, the values of the M^2 parameter are 1.75 and 1.5, respectively. It can be concluded that with the increase of the fiber lengths, the quality of the propagating light beam remains almost constant, i.e. the fiber supports single-mode beam propagation with the strong confinement at any length of the W-type delivery fiber. Thus, a remarkable feature of W-fiber is the high quality of preservation of the output beam with slight degradation along the length of the fiber 15 m. This is very good achievement for the delivery fiber, since usually the optimum fiber length where the beam quality remains unchanged does not exceed 1 - 2 m.

6.4 Optimal light launch system

The main and important task of fiber optics is the launching light beam into optical fibers, in other words, the introduction of light beam exactly into the fiber core so that most of light is directed along the fiber. Efficiently launching of a light beam into a fiber can be realized by forming a focus plane of the lens system exactly at the end of the fiber into which the light should be coupled. At the same time the beam diameter at the focal plane must match the MFD value of the fiber. This is possible to achieve by precise arrangement of free-space lens coupling system.

Essentially, a fiber launching system includes components such as a focusing lens in combination with optical fiber holder and control elements to fine adjust the input beam and focusing lens [10].

The starting point for arrangement of launching light system beam is carefully fixation of the optical fibers (the fiber pigtail of the radiation source and the W-type delivery fiber) in a special V-shaped groove with the clamps. Ideally, a check with a magnifying lens can be implemented to determine whether the end of the fiber is clean and intact. If the fiber has an angle cleave, then it will be more difficult to introduce the maximum possible power into such fiber, since any deviation from or roughness at the end of the fiber will change the required beam direction [10].

The next step is that the input beam is collimated by the lens with the corresponding beam diameter, and approximately aligned using the lens and the optical stage. To obtain high efficiency of light coupling into a fiber, it is necessary to estimate the collimated beam diameter after passing through the lens. It can be done from the mode field diameter (MFD) of the fiber pigtail and the focal length of the lens [10].

We have all necessary parameters (mode field diameter and divergence that was found in the previous section) to calculate the optical lens system for efficient light coupling; in other words, to establish beam apertures in an appropriate places. The mode field diameter (MFD)

and the divergence Θ for the fiber coming from the light emitting source and the Sample 1 of the W-type delivery fiber are presented in the Table 11 for a more convenient perception.

Table 11. The calculated mode field diameter and beam divergence for the fiber source and for the Sample 1 of the W-type fiber presented by two methods: "The 4 Sigma" and "The $1/e^2$ width"

	Mode field diameter, μm	Beam divergence θ, mrad
The calculation ***for the fiber source***	7.1669	186.1
1. The calculation by "The $1/e^2$ width" method ***for the W-fiber***	19.9141	68
2. The calculation by "The 4 Sigma" method ***for the W-fiber***	16.4097	82.9

The calculation of the optical lens system was carried out using special software. We need to choose a lens system that satisfies the values specified in the Table 11. The lens system forms a waist of the light beam and a divergence comparable with the values for the Sample 1 of the W-type delivery fiber obtained by "The $1/e^2$ width" and "The 4 Sigma" methods. For "The $1/e^2$ width" method, the MFD is 19.9141 μm and the beam divergence is 68 mrad; for "The 4 Sigma" method the MFD is 16.4097 μm and the beam divergence is 82.9 mrad, respectively.

As mentioned earlier, a radiating laser source designed for a wavelength of 1047 nm is connected to a single-mode fiber delivering a light beam having a Gaussian shape. The shape of a Gaussian beam with a given wavelength λ is determined by a single parameter that is called the beam waist ω_0 [53]. The beam waist is a measure of the beam diameter at the focal plane, where the beam width $\omega(z)$ is the smallest (and similarly, where the intensity is the largest), and can be obtained using a focusing lens. A light beam emerges from the single-mode optical fiber and passes through the lens, as a result the beam is focused on a spot, the diameter of which is the beam waist. Knowing the beam waist allows estimation of other

parameters including the Rayleigh length z_R and the asymptotic divergence of the ray θ. The Rayleigh length is the segment in which the waist of the light beam ω_0 increases $\sqrt{2}$ times, as shown on the Figure 46.

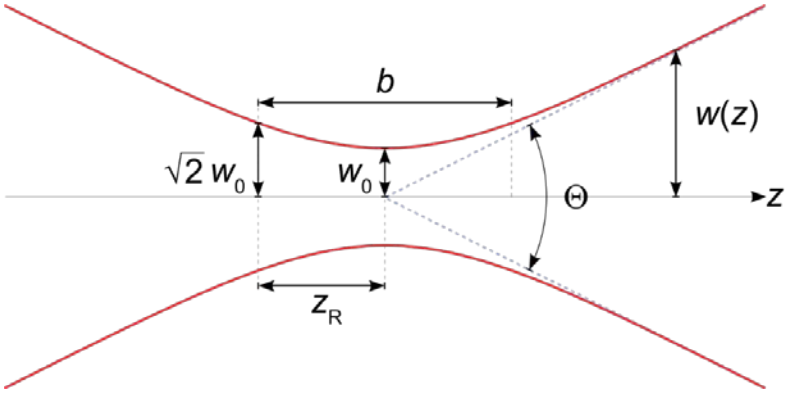

Fig. 46. Image of a light beam waist [53].

The beam waist can be calculated numerically using the equation [53]:

$$\omega_0 = \frac{2 \times \lambda}{\pi \times NA}. \quad (20)$$

Thus, we are faced with the task of selecting the lens system parameters to match the MFD and divergence of the laser source pigtailed fiber and the sample fiber. The condition for this is the following: after passing through the lens system, the light beam should have a beam waist less than the magnitude of the mode field diameter (MFD) of the Sample 1 of the W-type delivery fiber (values for the MFD for the Sample 1 of the W-type fiber are shown in the Table 11).

To select the appropriate lens system, it is convenient to use the software, a screenshot of which is shown in Figure 47. The optical lens system includes a set consisting of two lenses. The lenses were chosen according the lab availability. During the experiment the two sets of lenses were exploited with 25.4 and 75 mm of focal lengths and 50 and 100 mm of focal lengths. The first lens always forms a collimated beam, and the second lens realizes the beam focusing. Thus, by changing the distance between the lenses and optical fibers, it is possible to control the size of the beam waist and the beam divergence θ, thereby achieving the

necessary values close to the values indicated in the Table 11. Figure 46 shows a screenshot of a program that allows calculation of the optical system. In the upper left corner the yellow rectangles underline the values for the MFD of the light beam and the beam divergence θ for the fiber of the laser source. The numerical values circled in red ellipses are the focal lengths of the matched optical lenses - 25.4 mm and 75 mm, respectively. The numerical values circled in blue ellipses are the calculated distances between the optical fiber coming from the radiation source and the first lens (26.4 mm), between the first and second lenses (30 mm); between the second lens and the Sample 1 of the W-type fiber (67.1 mm) as shown in the Figure 47.

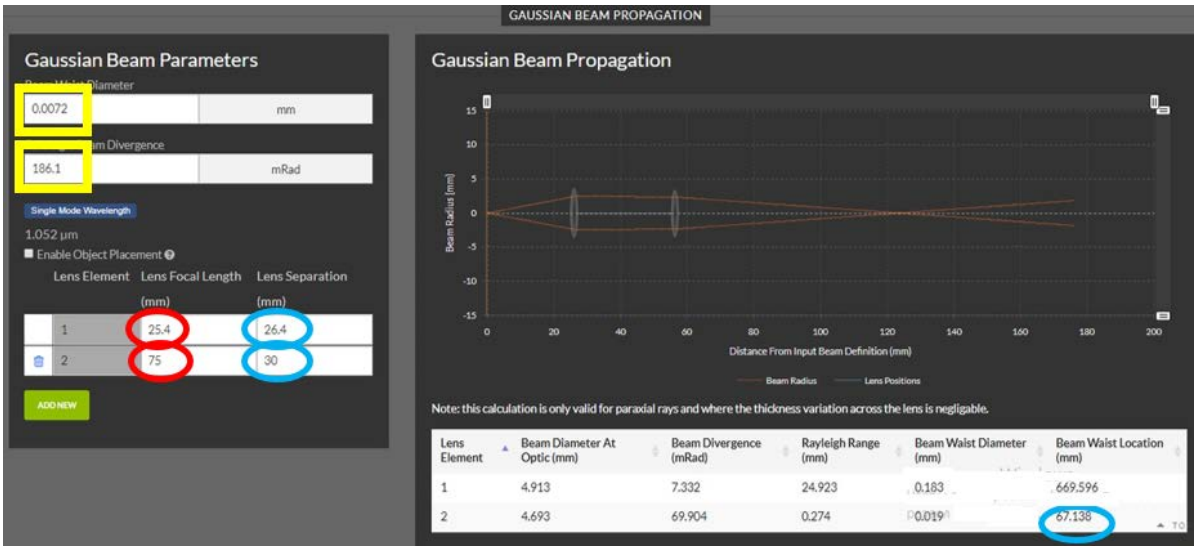

Fig. 47. Screenshot of the program to estimate the optimal position for the lenses with focal lengths 25.4 mm and 75 mm.

Using the calculation presented in Figure 47, the experimental setup for light coupling into a W-type delivery fiber was assemble. The photo of the setup is shown in the Figure 48.

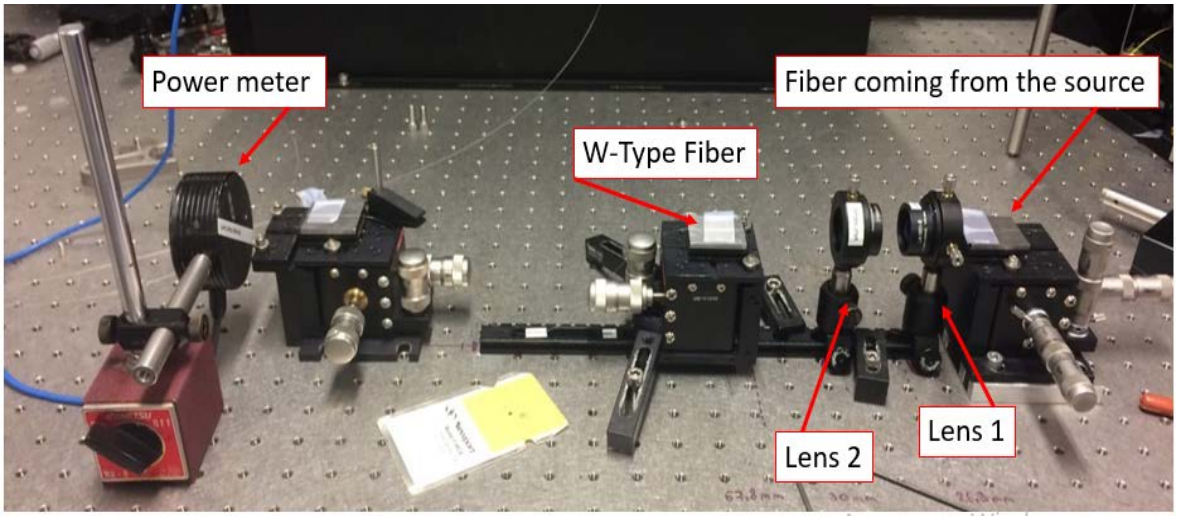

Fig. 48. An experimental setup for coupling light from a radiating source into a W-type fiber.

The experimental setup shown on the Figure 48 contains the following main components: a single-mode fiber pitail of the emitting laser source (on the right side in the Figure 48) mounted on the optical stage, two lenses, the first of which forms a collimated light beam, the second focuses the beam; and Sample 1 of the W-type fiber one end of which is placed on the optical stage (in the center); the other end is also mounted on the optical stage and locked into the power meter (on the left side).

As indicated earlier, the emitting laser source generates light at a wavelength of 1047 nm. The light coupled out passes through two optical lenses, the position of which is centered by the camera (this will be discussed below) so that the waist size of the focused beam corresponds to the mode field diameter (MFD). So, the first lens collimates light, the second lens focuses the radiation into a spot with the required beam waist size, and its focal point fall on the end of the Sample 1. The launch system efficiency is extimated via mesurement of the output optical power by power meter.

In order to match the micro-meter size of the MFD it is necessary to establish position of the lenses with respect to the single-mode optical fiber with high accurancy so that the diameter of the beam waist after passing through the optical lens system corresponds to the mode field diameter (MFD) of the sample. The accurancy of the lens positionining can be

ensured by measurement of the beam diameter using the camera and the far-field methods described earlier. This measurement gives information about the divergence θ of the beam passed through the lenses, as well as the diameter of the beam waist. A setup for measurement of the beam diameter after two lens system is shown in Figure 49.

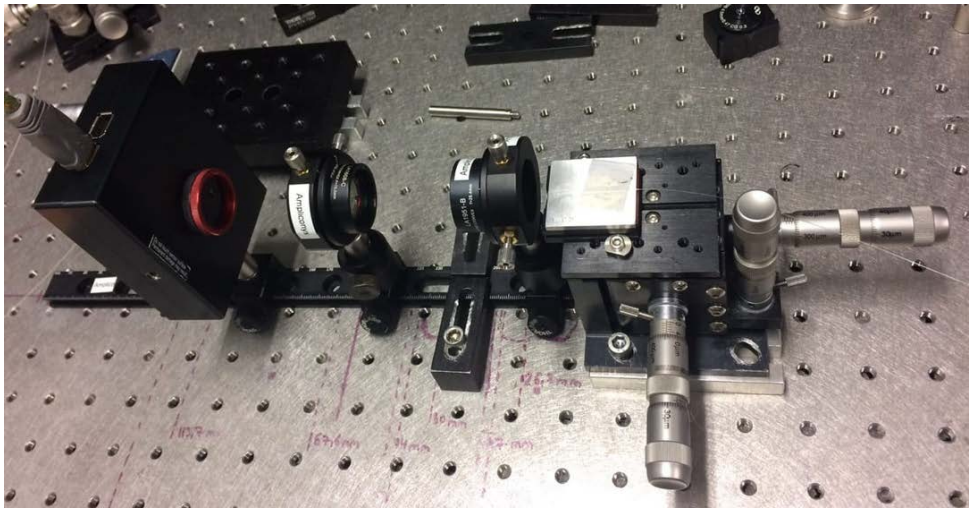

Fig. 49. An experimental setup for optical lens system assembly and verification.

Using the far-field measurement technique for the Sample 1, we obtained the measurements of the beam divergence Θ and MFD. The results are presented in the Table 12.

Table 12. Estimation of the divergence and the beam waist for optical lens system with focal lengths 25.4 mm and 75 mm by two methods: "The 4 Sigma" and "The $1/e^2$ width"

	"The 4 Sigma" method		**"The $1/e^2$ width"** method	
	X-value	Y-value	X-value	Y-value
Θ, mrad	81.3	77.3	85.6	80.4
Beam waist, μm	16.4054	17.2543	15.5813	15.5890

The values obtained for the diameter of the beam waist and the divergence indicated in the Table 12 are comparable to the values shown in the Table 11. The values calculated by "The 4 Sigma" method for a W-type optical fiber were 16.4097 μm and 82.9 mrad, which is the mode field diameter and the optical beam divergence θ, respectively. Therefore, we can conclude that the assembled optical system satisfies the condition for optimal coupling light into the fiber.

To understand how big percentage of the power we were able to inject from the emitting source into the W-type fiber, we need to measure the maximum power of the laser source. The radiation source power was 5.4 mW with a current value of 2.51 A.

It is known that light can propagate not only in the core of the optical fiber, but also in the cladding. Thus, in order to find the maximum possible power propagating along the fiber core only, it is necessary to remove the outer cladding and apply the polymer using an ultraviolet lamp. As described earlier, the cladding mode stripper helps to ensure that the modes propagating in the cladding go through the polymer into free space, into the air. Thus, modes are filtered and the distribution of modes is obtained primarily at the fiber core. The radiation output power transmitted through the W-type delivery fiber using the cladding mode stripper was 2.49 mW. This value is approximately 50% of the original laser source power.

The same procedure was applied to match the values corresponding to "The $1/e^2$ width" method. In the experiment, we used the same optical lenses with the focal lengths: 25.4 mm and 75 mm. The results are presented in the Table 12.

The values of the diameter of the beam waist and divergence are quite close to the values from the Table 11, which are 19.9 μm and 68 mrad, respectively. Consequently, the assembled optical system satisfies the condition for introducing light into the fiber.

With this lenses arrangement, an output power of about 1.89 mW was achieved. This is approximately 40% of the power of the original laser source. Such radiation power can be transmitted through a W-type delivery fiber.

The second set of lenses were characterized by 50 and 100 mm of the focal length. The calculation the corresponding lens position is shown in the Figure 50.

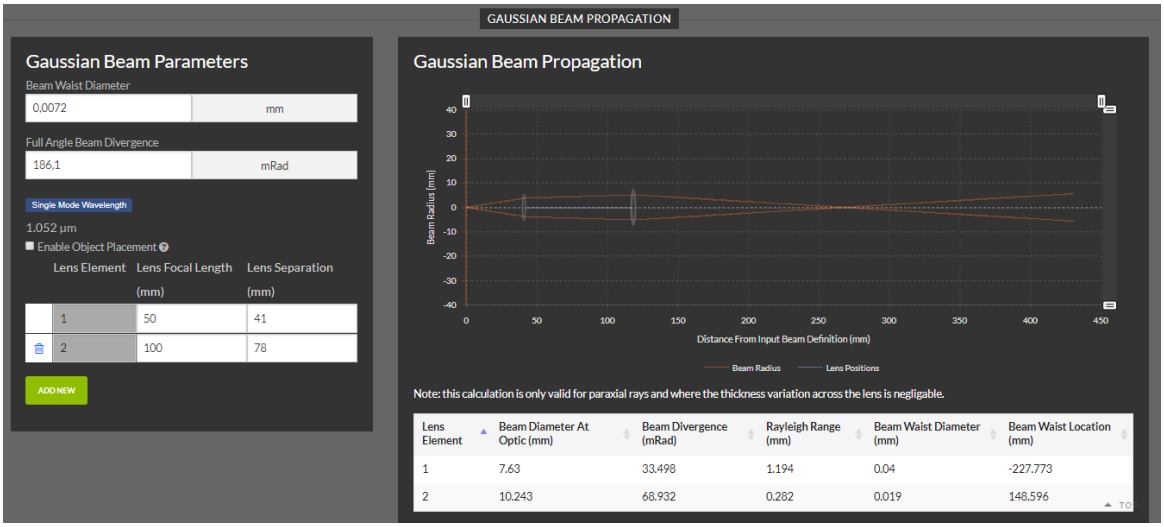

Fig. 50. Screenshot of the program to estimate the optimal position of the lenses with focal lengths 50 mm and 100 mm.

The whole measurement procedure is identical to the one described above for the first set of the lenses. The divergence of the light beam θ and the diameter of the beam waist after passing through a system of optical lenses are summarized in Table 13. As can be seen from the results, the values are similar to the values from the Table 11. The values calculated by "The $1/e^2$ width" method for a W-type optical fiber are 19.9141 μm and 68 mrad, which is the mode field diameter and the optical beam divergence θ, respectively. As a conclusion, the assembled optical system satisfies the condition for coupling light into the fiber, since the numerical apertures and the angular apertures approximately coincide. With this arrangement of lenses, the output power of about 1.68 mW was achieved. This is approximately 31 % of the power of the original laser source.

Table 13. Estimation of the divergence and the beam waist for optical lens system focal lengths 50 mm and 100 mm by two methods: "The 4 Sigma" and "The $1/e^2$ width"

	"The 4 Sigma" method		**"The $1/e^2$ width"** method	
	X-value	Y-value	X-value	Y-value
Θ, mrad	64.2	65.0	73.6	66.3
Beam waist, μm	20.7750	20.5194	18.1217	20.1170

The results for efficiency of coupling light into Sample 1 of a delivery W-type optical fiber from three experiments are summarized in the Table 14. As can be seen from the table the maximum efficiency obtained with the existing system was 50%, which is quite typical for a specific type of fibers. A possible improvement could be realized by development of a complex lens system to match even more precisely the mode field diameter and divergence of the W-type fiber.

Table 14. Summary of the output power measurements and lens system efficiency obtained from the experiments with Sample 1 of a W-type delivery fiber

	"The 4 Sigma" method	**"The $1/e^2$ width"** method	
Focal length lenses, mm	25.4 and 75	25.4 and 75	50 and 100
Power output, mW	2.49	1.89	1.68
Power source, mW	5.4		
Percentage of input power	50 %	40 %	31 %

7. CONCLUSIONS

In conclusion, this thesis focuses on the investigation of the novel W-type delivery fiber characterized by all-glass structure and large mode area. This fiber was developed to transfer ultra-short intense pulses generated by a solid-state laser. To satisfy the strict requirements for high-power pulsed system the delivery fiber must employ the following characteristics: large MFD, low sensitivity to the bending and high quality of the output beam ensuring only fundamental mode propagation in the fiber. All these characteristics were investigated for six samples of the W-type delivery fiber with the different geometry.

The high-power light from the laser is usually delivered to the workpiece in the laser-driven applications via an optical fiber. The fiber position is always moving to follow the required processing. As a consequence, the fiber might be bended all the time and the bending radius can be different. The experiments on the measurement of bending losses demonstrated that a large-mode area optical W-type delivery fibers are resistant to bending. The losses are only negligibly increased with a decrease of the bending radius. It is also a good indicator of the fundamental mode confinement in the fiber core.

The good quality processing is possible only with the perfect beam shape (for example Gaussian beam). Therefore, the delivery fiber should be capable to support only fundamental mode without quality distortion. The output beam quality determined by M^2 parameter is important characteristic of the delivery fiber. The measurements of the M^2 parameter were conducted for different lengths up to 15 m. According to the results, the beam quality demonstrated minor degradation with the increase of the fiber length. Therefore, a delivery fiber at least up to 15 m can be used in the processing. This is a very good achievement, since usually the length of a delivery fiber does not exceed a few meters.

The output of the high-power laser is usually presented by free-space optics due to specific of the CPA approach, therefore, the special lens system should be design for light coupling into a delivery fiber. In this thesis, two lenses setups were considered aiming to match precisely the MFD and the divergence of the fiber. The maximum efficiency of coupling system was as high as 50%. This is a relatively good results, which can be obtained

with the conventional lens system. The further improvement is possible with the special optics design, which will be the future goal of the work.

As a main conclusion, a W-type delivery optical fiber is an excellent tool for transmitting high-power optical radiation at least over 15 m length in a single-mode regime without beam degradation.

REFERENCES

[1] “ENCYCLOPEDIA BRITANNICA online.” https://britannica.com/.

[2] “Physics and radio-electronics. Characteristics of Laser.” https://physics-and-radio-electronics.com/physics/laser/characteristics-of-laser.html.

[3] J. Dutta Majumdar and I. Manna, “Laser material processing,” *Int. Mater. Rev.*, vol. 56, no. 5–6, pp. 341–388, 2011, doi: 10.1179/1743280411Y.0000000003.

[4] J. Berger, “Application of laser techniques to geodesy and geophysics,” *Adv. Geophys.*, vol. 16, no. C, pp. 1–56, 1973, doi: 10.1016/S0065-2687(08)60350-7.

[5] J.-T. Lin, “Progress of medical lasers: Fundamentals and Applications,” *Med. Devices Diagnostic Eng.*, vol. 1, no. 2, pp. 36–41, 2016, doi: 10.15761/mdde.1000111.

[6] Y. Hu, *Theory and Technology of Laser Imaging Based Target Detection*. Springer, 2017.

[7] D. C. Brown and J. W. Kuper, “Solid-State Lasers: Steady Progress Through the Decades,” *Opt. Photonics News*, vol. 20, no. 5, p. 36, 2009, doi: 10.1364/opn.20.5.000036.

[8] M. E. Fermann and Ingmar Hartl, *Ultrafast fibre lasers*. Nat.Photon, 2013.

[9] S. W. Oliver H. Heckl, Jochen Kleinbauer, Dominik Bauer and T. M. and D. H. Sutter, “Ultrafast Thin-Disk Lasers. Ultrashort Pulse Laser Technology,” *Book*, vol. 195, no. January, pp. 93–115, 2015, doi: 10.1007/978-3-319-17659-8.

[10] Dr. Rüdiger Paschotta, “RP Photonics Encyclopedia.” https://rp-photonics.com/encyclopedia.html.

[11] Y. Wang and H. Kan, “Optimization algorithm for the pump structure of diode side-pumped solid-state lasers,” Opt. Lasers Eng., vol. 45, no. 1, pp. 93–105, 2007, doi: 10.1016/j.optlaseng.2006.06.005.

[12] “The Operation of Optical Lasers and Modes. Thomasnet.” https://thomasnet.com/articles/automation-electronics/optical-laser-operations/.

[13] B. G. Bale and J. N. Kutz, “Variational method for mode-locked lasers,” *J. Opt. Soc. Am. B*, vol. 25, no. 7, p. 1193, 2008, doi: 10.1364/josab.25.001193.

[14] Clara J. Saraceno, Dirk Sutter, Thomas Metzger and Marwan Abdou Ahmed, “The amazing progress of high-power ultrafast thin-disk lasers,” *Journal of the European Optical Society*, vol. 15, no. 1, pp. 1–7, 2019, doi: 10.1186/s41476-019-0108-1.

[15] M. C. Falconi, D. Laneve, M. Bozzetti, T. T. Fernandez, G. Galzerano, and F. Prudenzano, “Design of an Efficient Pulsed Dy3+: ZBLAN Fiber Laser Operating in Gain Switching Regime,” *J. Light. Technol.*, vol. 36, no. 23, pp. 5327–5333, 2018, doi: 10.1109/JLT.2018.2871665.

[16] “How Fibre Lasers Work. Optoelectronics Research Centre. University of Southampton.” https://orc.soton.ac.uk/how-fibre-lasers-work.

[17] A. Klenke *et al.*, “22 GW peak-power fiber chirped-pulse-amplification system,” *Opt. Lett.*, vol. 39, no. 24, p. 6875, 2014, doi: 10.1364/ol.39.006875.

[18] Y. Wang and H. Kan, “Optimization algorithm for the pump structure of diode side-pumped solid-state lasers,” Opt. Lasers Eng., vol. 45, no. 1, pp. 93–105, 2007, doi: 10.1016/j.optlaseng.2006.06.005.

[19] T. Südmeyer *et al.*, “High-power ultrafast thin disk laser oscillators and their potential for sub-100-femtosecond pulse generation,” *Appl. Phys. B Lasers Opt.*, vol. 97, no. 2, pp. 281–295, 2009, doi: 10.1007/s00340-009-3700-z.

[20] V. E. Kisel *et al.*, “High-power, efficient, semiconductor saturable absorber mode-locked Yb:KGW bulk laser,” *Opt. Lett.*, vol. 40, no. 12, p. 2707, 2015, doi: 10.1364/ol.40.002707.

[21] V. Chvykov, R. S. Nagymihaly, H. Cao, M. Kalashnikov, and K. Osvay, “Design of a thin disk amplifier with extraction during pumping for high peak and average power Ti:Sa systems (EDP-TD),” *Opt. Express*, vol. 24, no. 4, p. 3721, 2016, doi: 10.1364/oe.24.003721.

[22] S. C. Kumar, G. Kumar Samanta, K. Devi, S. Sanguinetti, and M. Ebrahim-Zadeh, “Single-frequency, high-power, continuous-wave fiber-laser-pumped Ti:sapphire laser,” Appl. Opt., vol. 51, no. 1, pp. 15–20, 2012, doi: 10.1364/AO.51.000015.

[23] “Laser Safety Training Manual – Chapter 3. University of Toronto.” https://ehs.utoronto.ca/laser-safety-program/laser-safety-training-manual-b/.

[24] J.-N. Maran, P. Besnard, and S. LaRochelle, “Theoretical analysis of a pulsed regime observed with a frequency-shifted-feedback fiber laser,” *J. Opt. Soc. Am. B*, vol. 23, no. 7, p. 1302, 2006, doi: 10.1364/josab.23.001302.

[25] “Pulsed Lasers. Thorlabs manual.” https://thorlabs.com/images/tabimages/Laser_Pulses_Power_Energy_Equations.

[26] X. Li *et al.*, “Investigation of regime switching from mode locking to Q-switching in a 2 μm InGaSb/AlGaAsSb quantum well laser,” *Opt. Express*, vol. 26, no. 7, p. 8289, 2018, doi: 10.1364/oe.26.008289.

[27] J. Z. and Z. W. Junli Wang, Yupeng Xing, Lei Chen, Sha Li, Haotian Jia, “Passively Q-Switched Yb-Doped All-Fiber Laser with a Black Phosphorus Saturable Absorber,” J. Light. Technol., vol. 36, no. 10, pp. 2010–2016, 2018, doi: 10.1109/JLT.2018.2800910.

[28] J. Kim and Y. Song, “Ultralow-noise mode-locked fiber lasers and frequency combs: principles, status, and applications,” *Adv. Opt. Photonics*, vol. 8, no. 3, p. 465, 2016, doi: 10.1364/aop.8.000465.

[29] H. Yu, X. Wang, H. Zhang, R. Su, P. Zhou, and J. Chen, “Linearly-Polarized Fiber-Integrated Nonlinear CPA System for High-Average-Power Femtosecond Pulses Generation at 1.06 μm,” *J. Light. Technol.*, vol. 34, no. 18, pp. 4271–4277, 2016, doi: 10.1109/JLT.2016.2597862.

[30] C. J. S. de Matos, D. A. Chestnut, P. C. Reeves-Hall, and J. R. Taylor, “Continuous-wave-pumped Raman-assisted fiber optical parametric amplifier and wavelength converter in conventional dispersion-shifted fiber,” *Opt. Lett.*, vol. 26, no. 20, p. 1583, 2001, doi: 10.1364/ol.26.001583.

[31] H. H. Wahba and T. Kreis, “Characterization of graded index optical fibers by digital holographic interferometry,” Appl. Opt., vol. 48, no. 8, pp. 1573–1582, 2009, doi: 10.1364/AO.48.001573.

[32] “FiberLabs Inc. Optical fiber.” https://fiberlabs.com/glossary/optical-fiber/.

[33] D. C. S. Beddows, B. C. Griffiths, O. Samek, and H. H. Telle, “Devices To Analytical Laser Spectroscopy,” Appl. Opt., vol. 42, no. 30, 2003.

[34] “Snell’s Law.” https://eng.libretexts.org/Bookshelves/Materials_Science/Supplemental_Modules_(Materials_Science)/Optical_Properties/Snell’s_Law.

[35] R. Dändliker, “The concept of modes in optics and photonics,” vol. 3831, pp. 193–198, 2000.

[36] K. Igarashi, D. Souma, T. Tsuritani, and I. Morita, “Performance evaluation of selective mode conversion based on phase plates for a 10-mode fiber,” Opt. Express, vol. 22, no. 17, p. 20881, 2014, doi: 10.1364/oe.22.020881.

[37] K. Li, X. Chen, J. E. Hurley, J. S. Stone, and M.-J. Li, “High data rate few-mode transmission over graded-index single-mode fiber using 850 nm single-mode VCSEL,” *Opt. Express*, vol. 27, no. 15, p. 21395, 2019, doi: 10.1364/oe.27.021395.

[38] “Optical Fibres.” https://miniphysics.com/optical-fibres.html.

[39] “Gaussian Beam Propagation.” https://edmundoptics.com/knowledge-center/application-notes/lasers/gaussian-beam-propagation/.

[40] C. Ye, J. Koponen, V. Aallos, and T. Kokki, “Mode coupling in large-diameter multi-mode silica optical fibers,” Fiber Lasers X Technol. Syst. Appl., vol. 8601, p. 86012B, 2013, doi: 10.1117/12.2002819.

[41] N. G. R. Broderick, H. L. Offerhaus, D. J. Richardson, R. A. Sammut, J. Caplen, and L. Dong, “Large mode area fibers for high power applications,” Opt. Fiber Technol., vol. 5, no. 2, pp. 185–196, 1999, doi: 10.1006/ofte.1998.0292.

[42] X. Ma, C.-H. Liu, G. Chang, and A. Galvanauskas, “Angular-momentum coupled optical waves in chirally-coupled-core fibers,” Opt. Express, vol. 19, no. 27, p. 26515, 2011, doi: 10.1364/oe.19.026515.

[43] L. Dong, J. Li, and X. Peng, “ Bend-resistant fundamental mode operation in ytterbium-doped leakage channel fibers with effective areas up to 3160 μm 2 ,” Opt. Express, vol. 14, no. 24, p. 11512, 2006, doi: 10.1364/oe.14.011512.

[44] L. Bigot, Y. Quiquempois, A. Baz, and G. Bouwmans, “Pixelated high-index ring Bragg fibers,” Opt. Express, vol. 20, no. 17, p. 18795, 2012.

[45] H. T. Tomasz Nasiłowski, ElŜbieta Bereś-Pawlik, Francis Berghmans, Jan Wójcik, “Extremely large-mode-area photonic crystal fibre with low bending loss,” Opt. Express, vol. 18, no. 15, p. 15408, 2010, doi: 10.1364/oe.18.015408.

[46] Z. Liu, H. Y. Tam, L. Htein, M. L. V. Tse, and C. Lu, “Microstructured Optical Fiber Sensors,” *J. Light. Technol.*, vol. 35, no. 16, pp. 3425–3439, 2017, doi: 10.1109/JLT.2016.2605124.

[47] W. Wang et al., “Large mode area microstructured fiber supporting 56 super-OAM modes,” Opt. Express, vol. 27, no. 20, p. 27991, 2019, doi: 10.1364/oe.27.027991.

[48] “Large Mode Area Photonic Crystal Fibers.” http://fiber-lab.ru/new_ed/en/pcf_en.html.

[49] S. P. Singh and N. Singh, “Nonlinear effects in optical fibers: Origin, management and applications,” Prog. Electromagn. Res., vol. 73, pp. 249–275, 2007, doi: 10.2528/PIER07040201.

[50] S. P. Singh, R. Gangwar, and N. Singh, “NONLINEAR SCATTERING EFFECTS IN OPTICAL FIBERS S. P. Singh, R. Gangwar, and N. Singh,” Prog. Electromagn. Res. PIER, vol. 74, pp. 379–405, 2007.

[51] X. Fan, X. Ji, H. Yu, H. Wang, Y. Deng, and L. Chen, “Kerr effect on propagation characteristics of Hermite-Gaussian beams,” *Opt. Express*, vol. 27, no. 16, p. 23112, 2019, doi: 10.1364/oe.27.023112.

[52] W. M. K. Augusto Marcelli, Antonio Cricenti, Biological applications of synchrotron radiation infrared spectromicroscopy. 2012.

[53] “Wikipedia. The Free Encyclopedia” https://en.wikipedia.org/wiki.

[54] “Optical Fiber Preform Market.” https://egypt-business.com/ticker/details/1745-optical-fiber-preform-market---size-share-and-supply-with-competitive-landscape-2017-2021/178226.

[55] M. Y. Chen and Y. K. Zhang, “Bend insensitive design of large-mode-area microstructured optical fibers,” J. Light. Technol., vol. 29, no. 15, pp. 2216–2222, 2011, doi: 10.1109/JLT.2011.2158066.

[56] “OPTICAL FIBER LOSS AND ATTENUATION.” https://fiberoptics4sale.com/blogs/archive-posts/95048006-optical-fiber-loss-and-attenuation.

[57] N. Kaur and H. S. Parmar, “Non-linear scattering effects in fiber optic cables: a comprehensive review,” vol. 7, no. 11, pp. 217–226, 2016.

[58] D.Zangani, “Smart high-performance textiles for protection in construction and geotechnical applications,” Smart Text. Prot., pp. 276–305, 2013.

[59] “Laser Diode Technology.” https://newport.com/t/laser-diode-technology.

[60] “Ray theory transmission.” https://brainkart.com/article/Ray-theory-transmission_13602/.

[61] E. M. Kim and Douglas L. Franzen, Measurement of far-field and near-field radiation patterns from optical fibers. 1981.

[62] Photon Inc., “Measurement of Mode Field Diameters of Tapered Fibers and Waveguides for Low Loss Components,” Appl. Note, pp. 1–4, 2006.

[63] “Beam Quality.” https://edmundoptics.com/knowledge-center/application-notes/lasers/beam-quality-and-strehl-ratio/.